Analysis of damage to ship personnel in different seated postures by near-field underwater explosions

Kai Li[1]*, Shengbao Ding[1], Li Zhang[1], Zhijiang Yuan[2], Xiaogang Jiang[2], Yunlong Wang[1]

[1] School of Naval Architecture and Ocean Engineering, Dalian University of Technology, Dalian 116024, China
[2] Department of Navigation, Dalian Naval Academy, Dalian 116001, China

ARTICLE INFO

ABSTRACT

With the frequent occurrence of ship explosion accidents at sea, the safety of ships and crews has attracted much attention. At present, the research on crew injury is relatively weak. Consequently, the current study constructs a numerical model of the ship structure-crew-blast flow field to investigate the discrepancies in injury response of crew members across different sitting postures. LS-DYNA software is used for simulation and direct analysis to evaluate the damage of crew members in different positions under 100 kg TNT equivalent and 2 m blast distance conditions, and the relationship between different explosive equivalents and crew damage is analyzed. The results demonstrate that for crew members situated in working compartment, the injuries incurred across different sitting postures also differed. The lower leg and foot sections were at greater injury risks, while the head area was associated with minimal damage risks. Altering upper body postures of the crew human body had only a very small impact on lower extremity injuries. Moreover, positive correlations were exhibited between explosive equivalents and crew injury values. The research findings may offer references for injury analysis and protective device design of naval personnel.

1. Introduction

Ships are highly likely to be attacked by underwater weapons during their service [1]. Underwater explosions generated by underwater weapon attacks can be divided into near-field and far-field blasts, among which the destructiveness of near-field explosions is relatively higher. This is primarily attributed to the significant dynamic pressure effects of the shockwaves in near-field blasts, which exhibit substantial pressure attenuation. Underwater explosive will generate high temperature and high pressure bubble pulsating shock wave near the ship, which will act on the ship structure after propagation in the water and cause vertical impact

---

motion of the ship, thus damaging to the structure in different degrees [2]. Some researchers have explored the dynamic response of ship structure and equipment underwater explosion shock wave by means of experiments [3-5]. However, the cost of experiments is too high, and most scholars tend to use numerical calculation in the design stage. The main method in early research is double asymptotic method (DAA), which includes early high-frequency response and late vibration response [6]. Later, with the rapid development of finite element numerical method, a number of finite element software for calculating underwater explosions have been gradually derived, and researchers have conducted a large number of numerical simulation studies with the help of these software [7-8], further reducing the cost of research.

There are abundant research results on the damage response of ship structures in existing studies, but there are few analyses of damage to crew members in the destruction of ship structures. In terms of related research, many scholars have conducted studies on the damage to passengers after automobile explosion and collision. Researchers have used various finite element models of human body for analysis and exploration, and made judgments on the biomechanical response of passengers [9-10]. In the field of ship research, at the end of last century, relevant researchers have calculated the biological response of a single multi-rigid human finite element model caused by hull vibration [11], and Zong and Lam proposed a model of structure-human body interaction to study the biomechanical response of the ship personnel on board during the ship hull vibration caused by external impact [12]. Orlowski used a variety of finite element human body models to study the damage response of various parts of the human body in the process of ship collision, and analyzed the degree and risk of human damage [13].

The above studies focus on the dynamic response analysis of the ship structure in the case of underwater explosion, and less on the damage of the crew after the structural damage, and even less on the consideration of explosion damage and human posture. Therefore, based on the existing finite element model of human body, this paper establishes a numerical model including the crew, hull structure and blast flow field. The damage state of human body joints in different positions during near-field underwater explosion is analyzed to explore the damage response of underwater explosion shock waves to crew in the unrestrained system.

2. Crew human injury risk assessment index

Crew injury criteria are based on the degree of injury and risk that the damaged part of the human body can withstand. For the naval and maritime field, the currently obtainable relevant injury data are limited. However, considering that human tolerance to external impacts is confined and different external stimuli can lead to similar injury types, the crew injuries from underwater explosive shockwaves transferred through structures are analogous to those from collisions and mine blasts. Therefore, this study makes reference to standards in relevant fields, where the data are validated through experiments involving blasts, high-speed collisions and other aspects, demonstrating high reliability and wide applicability across different domains.

Subsequent crew injury risk evaluations are performed in the manner described in this section.

Table 1 The Abbreviate Injury Scale (AIS)

AIS Code	Injury Description
1	Minor
2	Moderate
3	Serious
4	Severe
5	Critical
6	Maximum (currently untreatable)
9	Unknown

The injury severity can be defined using injury scaling which is defined as the numerical classification of the type and severity of an injury. The most well-known anatomical scale, which is accepted worldwide, is the Abbreviated Injury Scale (AIS) (see Table 1).

2.1 Head

For the head, the U.S. Federal Motor Vehicle Safety Standards (FMVSS) have proposed the Head Injury Criteria (HIC), which is currently acceptable and most commonly used parameter for evaluating head injuries. The HIC is defined as follows:

$$HIC\left(\Delta t_{\max}\right) = \max_{t_1,t_2}\left[\left(\frac{1}{t_2-t_1}\int_{t_1}^{t_2}\hat{a}dt\right)^{2.5}(t_2-t_1)\right] \tag{1}$$

where $\hat{a}$ is the resultant acceleration of the head, and $t_2 - t_1$ is the interval during which the HIC value reaches the maximum value in the process of impact. The calculation time of the HIC value in the explosion condition is stipulated to be within 15 ms. In AEP-55 and TR-HFM-090 [14-15], the limit of HIC_{15} is 250. If HIC_{15} exceeds the limit, the occupant has a 10% or 5% chance of incurring moderate injury or more serious injury.

2.2 Neck

In FMVSS 208 final rule a neck injury criterion, designated N_{ij}, is used. The idea of the N_{ij} came from studies of Mertz [16] and Prasad [17], which lead to the conclusion that linear combination of tensile loads and extension could form the basis for an injury prediction function [18] .

This criterion is based on the belief that the occipital condyle-head junction can be approximated by a prismatic bar and that the failure for the neck is related to the stress in the ligamentous tissue spanning the area between the neck and the head. N_{ij} is defined as:

$$N_{ij} = \left|\frac{F_z}{F_{zc}}\right| + \left|\frac{M_y}{M_{yc}}\right| \tag{2}$$

where F_z and M_y are the axial force and the neck flexion–extension moment local to the occipital condyle as functions of time. F_{zc} and M_{yc} are normalization constants.

The N_{ij} calculation then consists in four calculations for the different loading modes. Eppinger [19] proposed N_{ij} Injury risk equations illustrated in Figure 1.
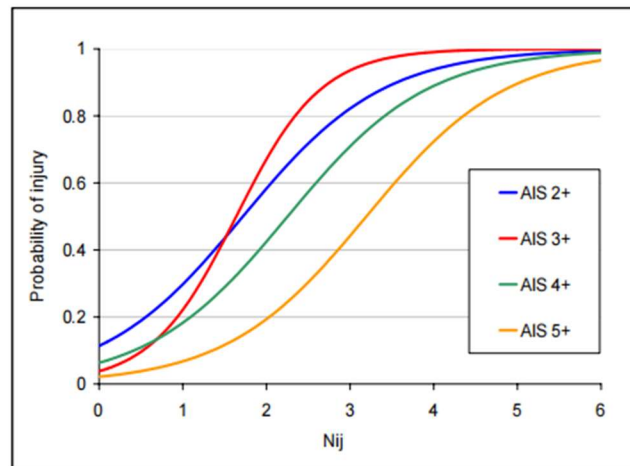

Fig. 1 N_{ij} risk curves

These curves are applicable to various dummy sizes to which different critical values are associated. According to [19], the thresholds for N_{ij}, F_{zc}, M_{yc} are used for the 50th percentile male Hybrid III:

$N_{ij} = 1$

$F_{zc} = 6860\ N$

$M_{yc} = 135\ N.m$

2.3 Thoracolumbar Spine

Stech and Payne [20] evaluated the Dynamic Response Index (DRI) as a general model to simulate the biomechanical response due to human body dynamics by using a single mass-spring-damper system (see Figure 2). The $DRIz$ is the Dynamix Response Index in axial direction (z-direction).
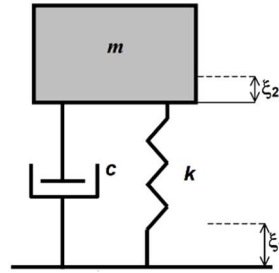

Fig. 2 $DRIz$ model

The equation of motion for this model is:

$$\ddot{z}(t) = \ddot{\delta} + 2 \cdot \varsigma \cdot \omega_n + \omega_n^2 \cdot \delta \tag{3}$$

where $\ddot{z}(t)$ is the acceleration in the vertical direction measured at the position of initiation; δ is the relative displacement of the system with $\delta = \delta_1 - \delta_2$, and $\delta > 0 \Rightarrow$ compression; ς is the damping coefficient with $\varsigma = \dfrac{c}{2 \cdot m \cdot \omega_n} = 0.224$; ω_n is the natural frequency with $\omega_n = \sqrt{\dfrac{k}{m}} = 52.9\, rad/s$.

The vertical dynamic response index ($DRIz$) was used to evaluate lumbar spine injury in AEP-55:

$$DRIz = \frac{\omega_n^2 \cdot \delta_{\max}}{g} \tag{4}$$

This formula shows that the relative maximum displacement $\delta_{\max}$ of the system can be obtained from the z-direction acceleration of the pelvis and the natural frequency of the system ω_n. The value of $DRIz$ can be calculated from the acceleration of gravity. TR-HFM-090 provides a lumbar spine tolerance of 17.7.

2.4 Tibia

Dynamic axial impact tests were conducted by Yoganandan [21], at the Medical College of Wisconsin (MCW). Experimentally derived risk equations for foot/ankle injuries, Figure 3 shows the probability distribution for foot/ankle injuries as a function of age and tibia force (peak value).

Based on the relation given on Figure 3, the probability of foot/ankle fracture can be expressed as follows:

$$p(fracture) = 1 - \left[\exp\left\{ -\left(\frac{0.0348 * age + 0.415 * F_T}{5.13076} \right)^{7.42582} \right\} \right] \tag{5}$$

where $p\left(fracture\right)$ is the probability of foot/ankle fracture; age is in years; F_T is the maximum tibia axial force value (in kN). According to [15], the tolerance level of F_T is 5.4kN. Using this Weibull probability equation presented above, the risk of foot/ankle fracture as a function of tibia force can be computed for any age.
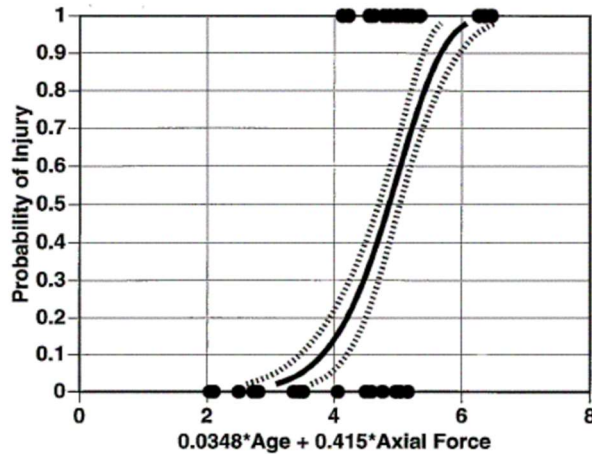

Fig. 3 Risk of foot/ankle injury as a function of age and tibia axial force

2.5 Femur

The test data (126 single impact tests using whole cadaveric subjects) reported by Morgan [22] was reanalysed using logistic regression for AIS 2+ and 3+ knee-thigh-hip injuries. The results of the analysis suggested that femur axial force alone was a reasonably good predictor of knee-thigh-hip injuries. The probability of knee-thigh-hip injuries as a function of applied femur force is presented in Equation 6, where F_E is the femur axial force. According to [19], the tolerance level of F_E =10 kN.

$$p\left(AIS\ 2+\right)=\frac{1}{1+e^{5.7949-0.5196F}}$$
$$p\left(AIS\ 3+\right)=\frac{1}{1+e^{4.9795-0.326F}} \tag{6}$$
$$F_E = femur\ axial\ force$$

In summary, all the injury assessment metrics adopted in this study have been briefly introduced, and Table 2 summarizes the threshold values and corresponding injury risk levels of each metric.

Table 2 Injury criteria and extremes for different parts of the body

Parts	Injury Indicators	The threshold corresponds to the damage risk	Damage Threshold
Head	HIC_{15}	10% AIS2+	250
Neck	F_{zc} (kN)	10% AIS2+	6.86
	M_{yc} (N.m)	relative safe	135
	N_{ij}	10% AIS2+	1
Thoracolumbar Spine	$DRIz$	10% AIS2+	17.7
Tibia	F_T (kN)	10% AIS2+	5.4
Femur	F_E (kN)	10% AIS2+	10

3. Calculation model building and calibration

3.1 Assumed explosion scenario

Taking a small fishing administration vessel as the object of study, the ship has a length of 66.5 meters, a width of 8.5 meters, a depth of 4.3 meters, a displacement of 857 t. The frame spacing is 0.5m. There are 7 transverse bulkheads in the ship.

The finite element model was developed to facilitate simulations of explosion impacts that cause large deformations; hence, the whole ship was included as shown in Fig. 4(a). The plate thickness of the ship hull and internal structures was 6-12 mm. Because the structures are expected to be in direct contact with the explosion wave, the ship is modeled in detail to accurately represent the actual structural strength. As shown in Fig. 4(b), the shell panels, internal decks, bulkheads and web frames are carefully modeled by using shell elements, and the longitudinals, stiffeners are modeled by using beam elements.

To analyze the extent of crew injuries from underwater blasts under adverse conditions, the fishing administration office, which is the compartment right above the explosion source, was selected for case analysis in this study. If the crew members inside the compartment nearest to the explosion source remain non-fatally injured, personnel in other cabins (such as the wheelhouse, meeting room, living room, etc.) will also be in a safe status under the same conditions.

To sufficiently simulate the crew injury scenarios and minimize interferences from other factors, shell element was adopted in this study to simulate the seats, which are treated as the medium transferring blast loads between the structure and the crew human body. Hui, Hadi and Mikulee mentioned the specification of hull structure grid and watershed grid [23-25]. Among them, Lagrange grid is adopted for hull and seat structure, Euler grid is adopted for explosion flow field (air, water and explosives), the size of Euler domain is 80m×17m×25m, and the thickness of air layer above water is 10 m, as shown in Fig.4(c). The seats, deck and shell plating were modeled with Belytschko-Tsay shell elements using a mesh size of 100 mm, while beam elements were used for other ship structural members with finer meshes for transition. The fluid domains (including air and water) were discretized by Solid163 elements with a mesh size of 200 mm.

Compared with the ship damage caused by underwater weapons in relevant literature, more severe blast conditions were selected in this study, specifically by positioning the explosion source right beneath the ship hull. According to the compiled data on the TNT equivalents of sea mines from various countries by Szturomski [26], this study selects an explosion depth of 2 m and 100 kg TNT equivalent as the blast source parameters, to be utilized in subsequent numerical simulation analyses. The explosive is assumed to be under the engine room, as shown in Fig.4(d). The hull shock factor (HSF) is employed to describe intensity of the shock wave [27]. The HSF is determined as

$$C_{HSF} = \frac{\sqrt{M}}{R} \tag{7}$$

where M is the weight of explosion in TNT equivalence (kg); R is the stand-off distance from the charge to the target (m). In this study, the HSF is set to be 5.

The model configuration for the blast loading is illustrated in Figure 4. The coupling relationship is defined between the ship structure and the blast flow field, the contact relationship is defined between the crew and the deck and the seat, the friction coefficient is 0.2, and the self-contact is defined between the hull structures. Calculations are performed using the R11.1.0 single-precision solver in LS-DYNA.

The 50th percentile male HYBRID III human finite element model is adopted to simulate the human body of the crew, which has been validated to accurately evaluate the degree of damage to the human body under vertical impact loading [28]. Therefore, when used to investigate the damage to the head, neck, thoracolumbar spine, tibia and other parts of the body, it can better simulate the damage to various parts of the body of the crew after suffering from underwater explosions.
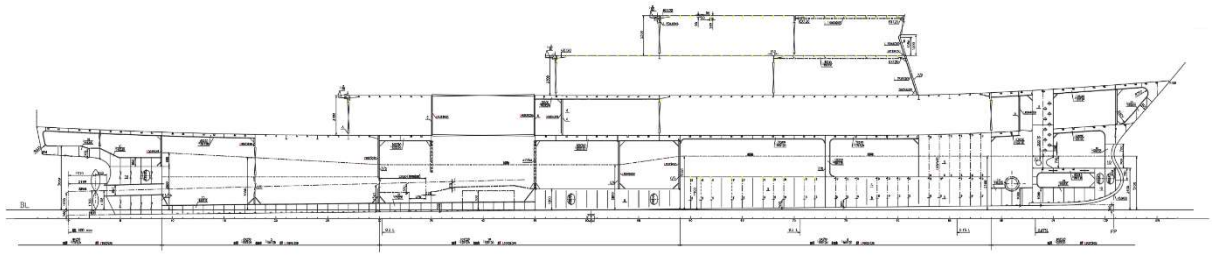
(a) Drawing of ship structure
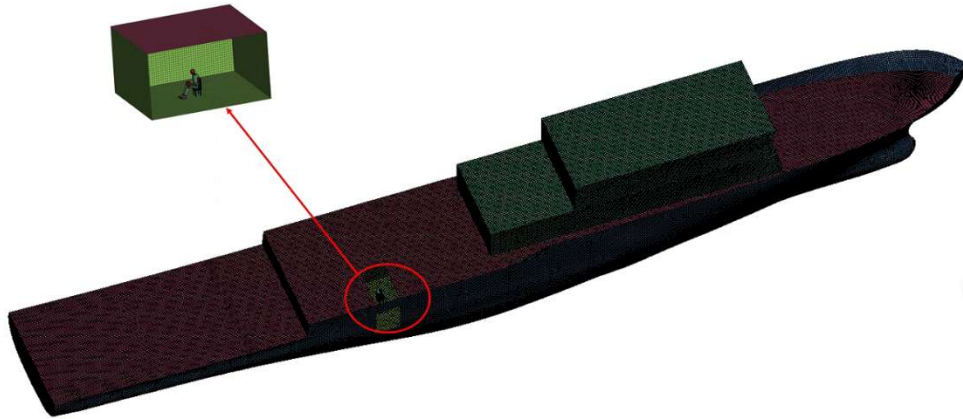
(b) Finite element model of ship structure
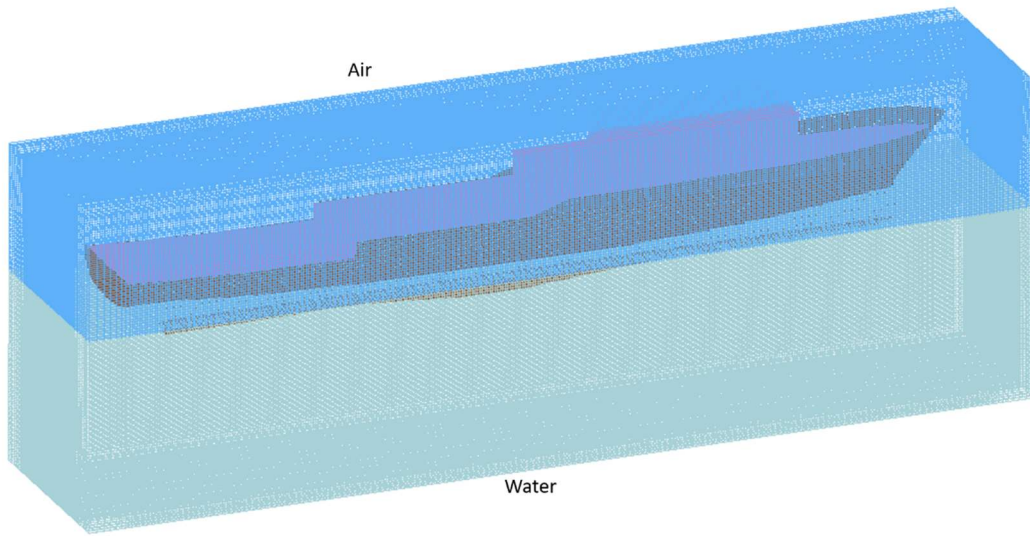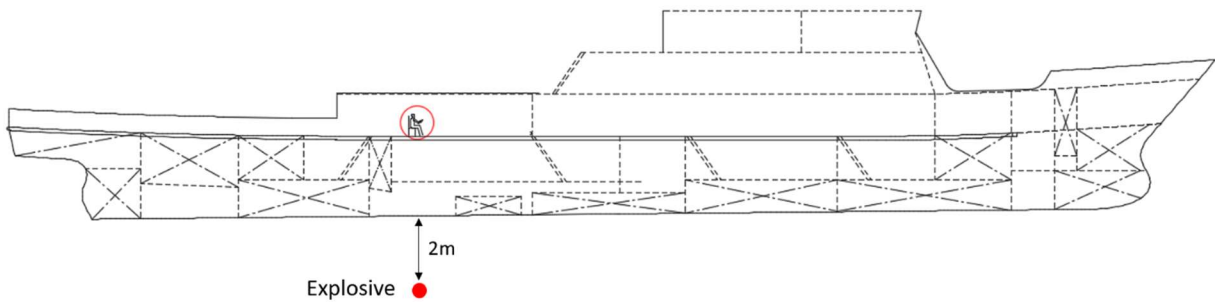

(c) Structure-dummy-fluid coupling model

(d) Near-field underwater explosion scenario

Fig. 4 Finite element modelling and explosion scenario

3.1.1 Hull material model

To simulate the material properties of the compartment, the shell element with grid size of 200 mm and Q235 steel is adopted. The steel has a modulus of elasticity of 210 GPa, a Poisson's ratio of 0.3, a yield strength of 235 MPa, and a failure strain of 0.3 [29]. The Cowper-Symonds intrinsic model is used to represent the stress-strain relationship for materials subjected to strain rate under dynamic loading:

$$\sigma_y = \sigma_0[1+(\frac{\dot{\varepsilon}}{D})^{1/P}] \tag{8}$$

where $\dot{\varepsilon}$ is the strain rate; σ_y is the stress value corresponding to $\dot{\varepsilon}$; σ_0 is the stress value in the static case; D and P is material constants, $D = 40.5$, $P = 5$.

3.1.2 Air

Air is modelled by the material type Mat_Null with a specific Linear Polynomial EOS, and this EOS is expressed as LSTC:

$$P = C_0 + C_1\mu + C_2\mu^2 + C_3\mu^3 + (C_4 + C_5\mu + C_6\mu^2)E \tag{9}$$

where P is the pressure of air, E is the internal energy per volume, μ defines the compression of air by $\mu = (\rho/\rho_0)-1$ with ρ and ρ_0 being the current and initial density of air, respectively. C_0, C_1, C_2, C_3, C_4, C_5 and C_6 are material constants of air, and C_4 and C_5 are equal to 0.4. The parameters for air are well documented with previous experimental calibrations and listed in Table 3.

Table 3 Air material model and state equation parameters

ρ (kgm^{-3})	C_0, C_1, C_2, C_3, C_6	C_4, C_5	E (GPa)
1.29	0	0.4	2.53e^{-4}

3.1.3 Water

Water is modeled by the material type of Mat_Null combined with the Gruneisen EOS [30], and this combination is widely used for simulating water-filled blasting and underwater explosion. The parameters for water are also well documented with previous experimental calibrations and listed in Table 4.

$$P = \frac{\rho_3 c^2\mu[1+(1-\frac{\gamma_0}{2})\mu-\frac{\alpha}{2}\mu^2]}{[1-(S_1-1)\mu-S_2\frac{\mu^2}{1+\mu}-S_3\frac{\mu^3}{(1+\mu)^2}]^2} + (\gamma_0+\alpha\mu)E_1 \tag{10}$$

where P is the pressure of water, γ_0 is the Gruneisen gamma, α is the first order volume correction to γ, and μ is equal to $(\rho/\rho_0)-1$ with ρ and ρ_0 being the current and initial density of water, respectively; c is the speed of wave propagation in water, $c = 1500m/s$; E_1 the internal energy per unit volume, S_1, S_2 and S_3 are the coefficients, respectively. The parameters for the equation are listed in Table 4.

Table 4 Material model and equation of state parameters for water

S_1	S_2	S_3	γ_0	α	E_1 (GPa)
2.56	1.98	1.23	0.50	0.00	1.01e^{-4}

3.1.4 Explosive

In LS-DYNA, the material type of Mat_High_Explosive_Burn together with EOS of Jones–Wilkins–Lee (JWL) is widely used to simulate the pressure generated by the expansion of detonation products [31,32]. This JWL EOS defines the detonation pressure P_e in the form of Lee [33]:

$$P_e = A_e(1-\frac{\omega}{R_1 V_e})\mathrm{e}^{-R_1 V_e} + B_e(1-\frac{\omega}{R_2 V_e})\mathrm{e}^{-R_2 V_e} + \frac{\omega E_e}{V_e} \tag{11}$$

where V_e is the relative volume of the detonation product, E_e is the detonation energy per unit volume with an initial value of E_{e0}, and A_e, B_e, R_1, R_2 and ω are explosive constants. Generally, the parameters for explosive are determined based on the specifications of explosive. In the current modelling, the parameters for explosives used in blasting tests are obtained in Banadaki tests [34] and listed in Table 5.

Table 5 Explosives-related parameters

ρ_e (kg/m3)	E_e (GPa)	A_e (GPa)	B_e (GPa)	R_1	R_2	ω
1630	7.17	374.2	3.23	4.15	0.9	0.3

3.2 Dummy different posture models

3.2.1 Initial posture

The dummy model adopted in this study is the 50th percentile rigid seated dummy provided by the LSTC (Livermore Software Technology Corporation) official website, which has been extensively applied in automotive blast and collision injury research, with its accuracy validated through experiments. The sitting position is a typical working status of most crew onboard, this paper only analyzes the sitting model with different postures.

Considering the real onboard state of the human body, the initial posture is shown in Figure 5 below: the dummy's feet are placed on the deck surface, the arms are perpendicular to the back, the pelvis and lumbar area are in contact with the seat, and the original posture used by Livermore Software Technology Corporation (LSTC) when developing the dummy is used for the neck. In order to avoid the impact of the seat cushion, energy-absorbing structure and other factors to the dummy by the explosion, the seat is selected without any cushioning mechanism of the rigid seat, the seat is fixed to the deck through the CONSTRAINED_EXTRA_NODES keyword.
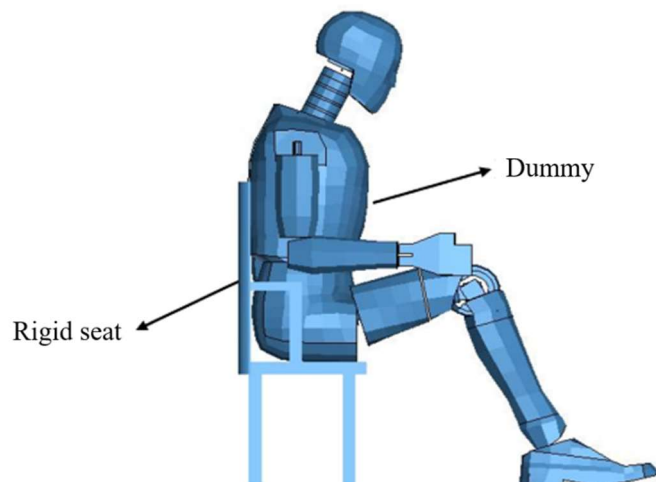

Fig. 5 Initial posture of the dummy

3.2.2 Initial posture Change of joint angle posture

The posture of the crew in the cabin is random. In order to simulate the injury of the crew in different possible postures under the explosion situation, the posture of the dummy 's foot, tibia, femur, waist, elbow and wrist is changed at different angles by referring to the variable posture determined in ergonomics [35]. Five angle parameters are controlled: the angle between foot and tibia (M_1), the angle between tibia and femur (M_2), the angle between femur and waist (M_3), the angle between waist and elbow (M_4), the angle between elbow and wrist (M_5), as shown in Figure 6 below:
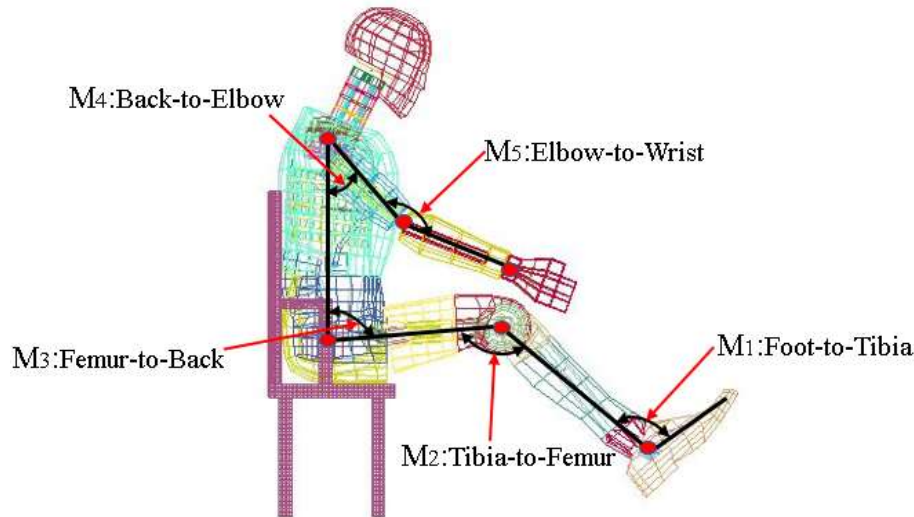

Fig. 6 The Dummy Changes the Joint Posture

At the same time, the angle changes of each joint should be controlled reasonably. The range of changes is shown in Table 6.

Table 6 Range of variation by joint

Joint Angle	Angle change range (°)		
Foot-to-Tibia (M_1)	110	95	105
Tibia-to-Femur (M_2)	90	80	105
Femur-to-Waist(M_3)	70	65	80
Waist-to-Elbow (M_4)	0	5	15
Elbow-to-Wrist (M_5)	90	100	110

3.2.3 Constraint of local joint posture

In order to study the influence of underwater impact on the crew under local joint constraints, other conditions are kept unchanged. Based on the initial model, the constraints of tibia and foot joints are applied to the dummy to explore the influence of tibia and foot motion on the crew 's injury response. The constraint conditions are shown in Figure 7 and Figure 8. In the actual operation of self-protection under blast wave, the crew should take some efforts to avoid flying off the deck after being impacted, this study limits the tibial freedom of the dummy during the simulation.
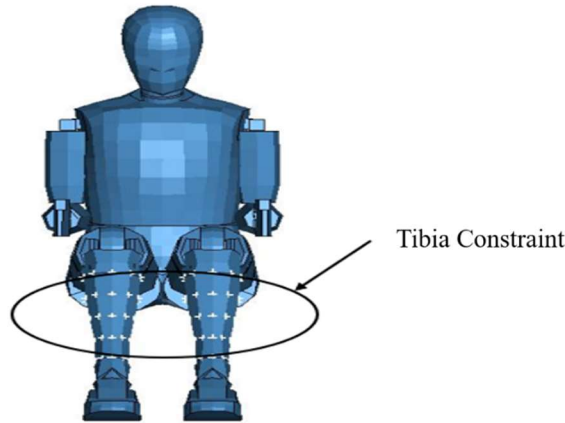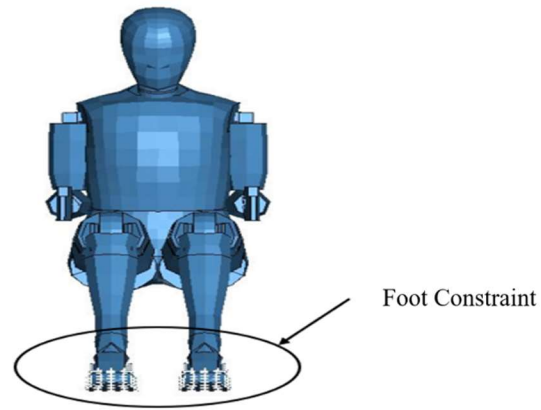
Fig. 7 Dummy tibia constraint   **Fig. 8** Dummy foot constraint
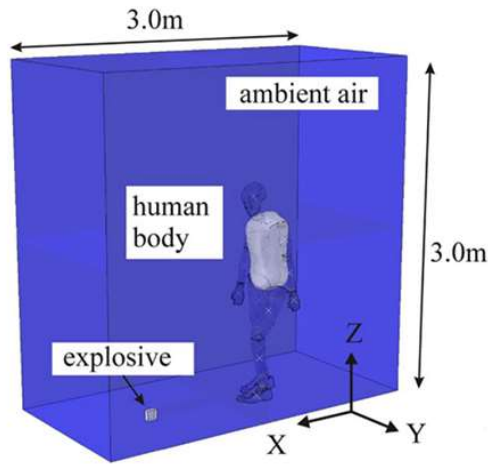
3.3 Numerical simulation method calibration

3.3.1 Verification of ALE numerical method

Underwater explosion is a typical fluid-solid interation (FSI) problem. As for the processing of FSI problem, it has been realized that Eulerian numerical method is accurate and well-tested to simulate high-speed flows, and that Lagrangian numerical method is suitable for addressing material responses to the loading and deformation [32]. Arbitrary Lagrangian Eulerian method (ALE) combines the advantages of both and improves the accuracy of numerical simulations. Studies investigating ship structure and human subjects simultaneously are scarce in current literature, most of current researches evaluate the impacts of explosions on ship structures only, whereas the focus on human injury analysis caused by underwater explosion are few. The available related studies merely analyzed the effects of shockwaves under air blast conditions of TNT on the human body. Based on these references, this study conducts a validation analysis at first.

In order to verify the effectiveness of the numerical method, the model mentioned by Sielicki and Gajewski [36] is used for analysis, which is shown in Figure 9 (a). According to the parameters in this paper, a cubic air domain with a side length of 3 m is established. The grid size of the air domain is 20 mm. The human body model and the explosive are placed on both sides of the air domain. In this paper, one of the working conditions is selected for analysis and calculation. The explosive equivalents used are 0.4 kg, 0.6 kg, 0.8 kg, and 1.0 kg, respectively. The distance between the explosive and the human body model is 1m. All parameters are the same as those in the literature, and the non-reflective boundary conditions are set on the outer surface of the air, simulating an infinite field. After the calculation is completed, the pressure in the air domain at 0.05 m in the normal direction of the ear surface of the human body model is extracted and compared with the literature results. Table 7 shows the error comparison between the numerical simulation values and the literature results, the simulation results have a small error with the literature values.

Table 7 Pressure results at 0.05 m in the direction normal to the surface of the left ear of the manikin

Burst distance (m)	Explosive equivalent (kg)	Literature results (MPa)	Numerical simulation values (MPa)	Relative error (%)
1	0.4	276.1	273.6	-0.90
1	0.6	344.1	341.8	-0.67
1	0.8	380.5	381.2	0.18
1	1.0	419.9	418.4	-0.36

(a) Geometry of the domains including the obstacle body, ambient air and explosive [36]
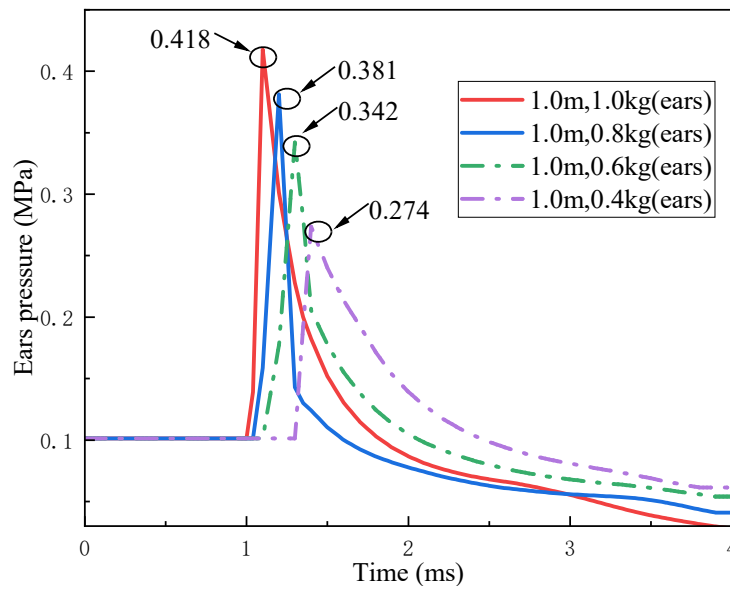
(b) Pressure time course curve at the position corresponding to different explosive equivalents
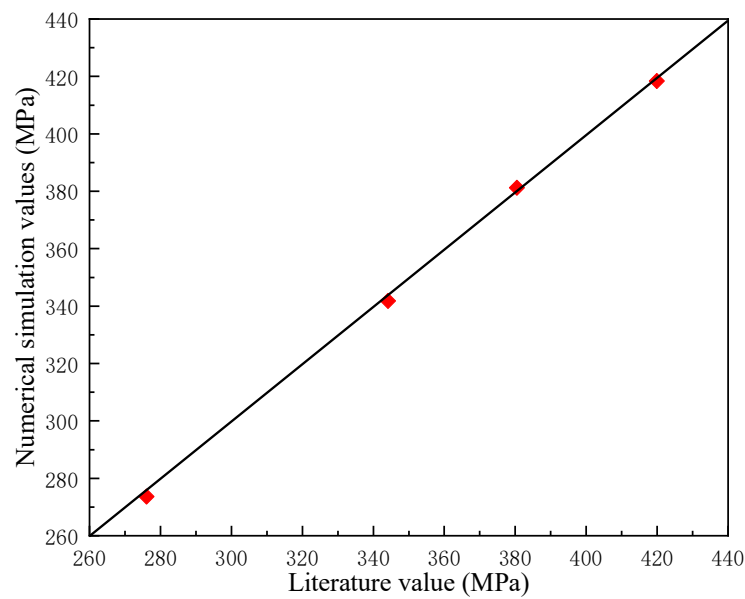
(c) Corresponding values of numerical simulation results to literature results

Fig. 9 Comparison of numerical method validation

Figure 9 (b) is the pressure change curve of the left ear of the human body model at the same detonation distance and four kinds of explosive equivalent. It can be seen that the greater the explosive equivalent, the faster the pressure peak appears. On the contrary, the pressure peak will be delayed backwards and the peak becomes smaller. The overall change trend of the curve is the same as that in the literature. Figure 9 (c) compares the literature results with the numerical results. It is seen that the points are close to the line of perfect match, suggesting reasonable agreement between literature and FE simulation. According to the above results, the numerical simulation method in this paper is accurate enough to analyze the dynamic response of the human body model.
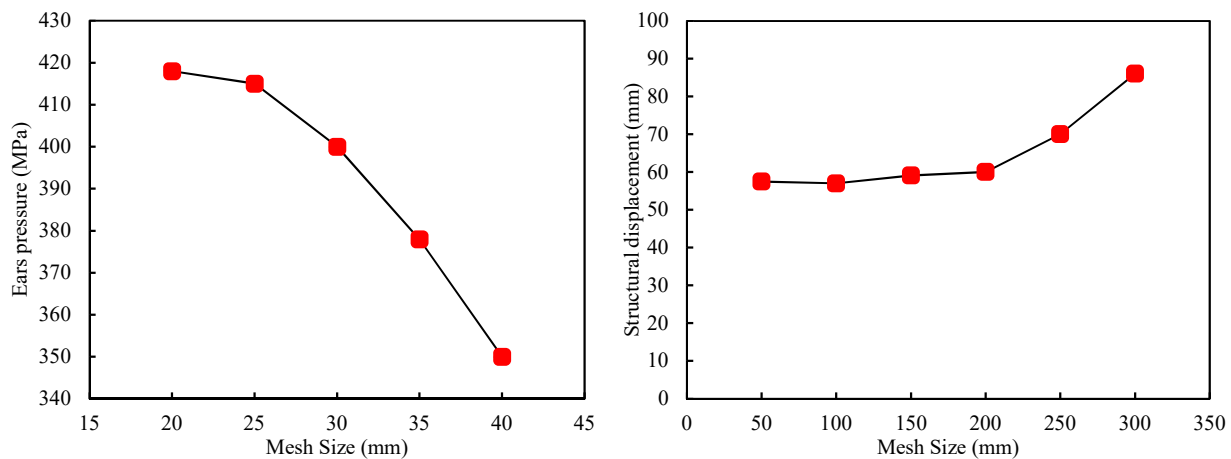
3.3.2   Grid sensitivity analysis

The mesh size of the Euler domain has a great influence on the finite element simulation results. Therefore, it is necessary to study the convergence of the mesh to determine the element size in the numerical model. Using the numerical model established above, under the same other conditions, the grid size gradually increases from the first 20 mm, and the pressure values at the corresponding positions of 25 mm, 30 mm, 35 mm and 40 mm grids are calculated respectively. From Figure 10(a), it can be seen that when the grid size changes from 20 mm to 25 mm, the difference of the pressure peak at the corresponding position is small. When the grid size is greater than 30 mm, the difference between the pressure peak and the literature results becomes larger. It can be seen that when the grid size is less than or equal to 25 mm, the calculation results converge, the model runs stably and reasonably. Therefore, when analyzing the human body model later, the local grid size is selected to be 25 mm, and the grid setting of the farther position is gradually changed. The overall performance is sparse around and encrypted in the middle.

To assess the mesh impact on results and improve computational efficiency, a densified intermediate and sparse peripheral mesh was adopted in this study, with intermediate mesh size varying from 50 to 300 mm. As shown in Figure 10(b), the results show that when the intermediate flow field mesh size is less than or equal to 200 mm, the discrepancies in results are minor, whereas larger deviations are exhibited at sizes greater than 200 mm. Therefore, considering computational resource savings, a flow field (including air and water) mesh size of 200 mm was selected in this study, which can yield relatively accurate results.

(a) Peak pressure corresponding to different mesh sizes   (b) Structural displacement corresponding to different mesh sizes

Fig. 10 Response values under different mesh sizes

Based on the grid sensitivity analysis, in total, 2362800 solid elements were used to model the flow field, 293568 shell elements and 82861 beam elements were used to model the ship structure, and 34525 shell elements were used to model the dummy, and 648 shell elements were used to model the seat.

4. Simulation results

To rapidly determine the crew status, only the injuries from the first shockwave impact were considered, without accounting for the bubble pulsation effects. The calculation type is explicit, the duration is set to 60 ms, and the time step is the default value.

4.1 Response of ship structure

Fig.11 shows the stress and deformation of the ship structure at several different time points in the process of suffering from explosion wave. This sufficiently indicates that blast shockwaves can impose substantial vibrations and impacts on the hull, along with certain deformations in internal components. It is thus evident that the localized accelerations resulting from the explosion can load the crew members and lead to injuries of varying extents. The entire ship moves upwards, and strong localized deformations can be observed.

A roughly circular region of bottom was stressed at first, and the stress travelled very quickly. Initially, the plating in the centre of the ship section began to bow inward under the pressure of the shock wavefront, but the shape of the envelope of stressed plating was influenced by the pattern of stiffening under the plate.

As time passed, the stress continued to travel outward through the structure, loading the upper side shell and the higher decks. Figure 11 demonstrates this process. The side shell slid upwards and transferred load to the upper decks. The contour plot of the (von Mises) equivalent stress reveals the high stresses in the impact region.

(a) 8 ms

(b) 10 ms

(c) 16 ms
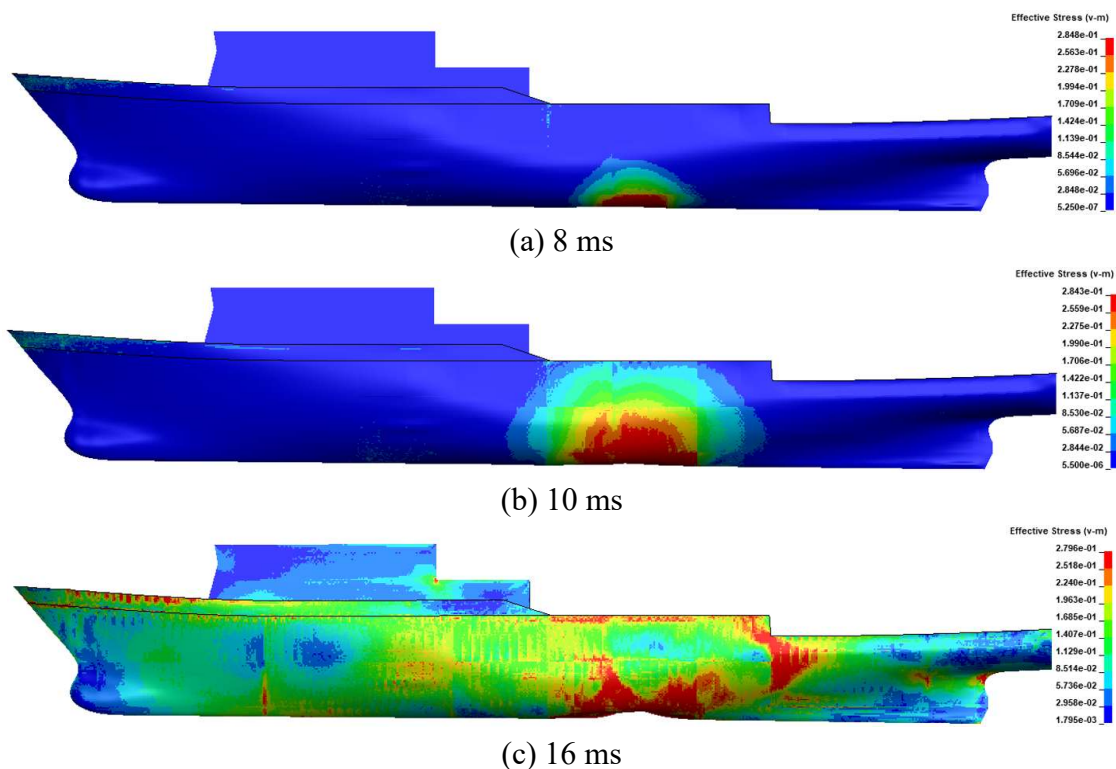
Fig. 11 Response of ship structure under near-field underwater explosion

4.2 Initial posture damage analysis

As shown in Fig.12, the way the crew suffers from the shock wave load mainly comes from two aspects. One is the part where the pelvis contacts the seat, and the other is the part where the foot contacts the deck. The occupants are subjected to upward impact loads through these two parts, resulting in upward acceleration. According to the calculation results, the head, pelvis, lumbar spine, tibia and other parts with serious human injury under vertical impact load are selected for analysis.

```
                          ┌──────────────┐
                          │ Shock wave   │
                          └──────┬───────┘
                                 │
                          ┌──────┴───────────┐
                          │ Deck acceleration│
                          └──────┬───────────┘
                    ┌────────────┴────────────┐
              ┌─────┴──────┐           ┌───────┴──────┐
              │    Seat    │           │    Foot      │
              └─────┬──────┘           └───────┬──────┘
                    │                   ┌──────┴──────┐
                    │                   │   Tibia     │
                    │                   └──────┬──────┘
                    │                   ┌──────┴──────┐
                    │                   │   Femur     │
                    │                   └──────┬──────┘
                    └────────────┬────────────┘
                          ┌──────┴───────┐
                          │   Pelvis     │
                          └──────┬───────┘
                          ┌──────┴───────┐
                          │ Lumbar spine │
                          └──────┬───────┘
                          ┌──────┴───────┐
                          │    Neck      │
                          └──────┬───────┘
                          ┌──────┴───────┐
                          │    Head      │
                          └──────────────┘
```
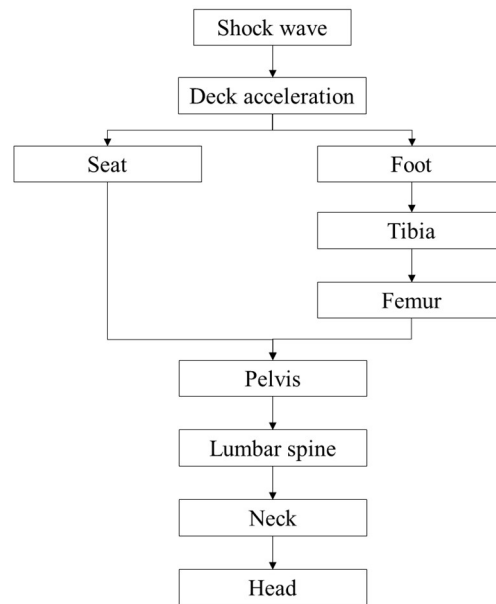
Fig. 12 The transmit path of shock wave load within the human body

According to the analysis of the motion process of the dummy in Figure 13, it can be seen that the dummy moves upward with the hull structure under the action of the shock wave generated by the underwater explosion. At 8ms, the dummy foot reaches maximum compression in the vertical direction, and as the deck continues to transmit the load, the dummy foot begins to separate from the deck at 10ms and is not subject to impact damage from it until the foot next falls back to the deck. Under the impact of the seat acceleration, the pelvis of the dummy began to move upward from the seat at 16ms, which lasted for about 20ms. Then, under the action of gravity, the dummy fell back to the seat and the deck again. Moreover, at 30ms, the femur of the dummy had moved above the wrist and the arm continued to move downward. After the dummy fell back to the seat and the deck above, under the continuous impact of deck acceleration, the lower torso of the dummy began to produce large deformation at 40 ms, and the left and right sides of the tibia and foot began to move towards each other, with the tendency of lateral turning and concave, while the waist of the dummy gradually bent downward in a compressed state. Finally, under the action of inertia force and the adjustment of the dummy itself, the tibia and femur of the dummy were gradually stretched horizontally at 49 ms to slow down the damage caused by the shock wave.

In order to evaluate the specific damage of each part of the dummy, the damage curves of each part of the dummy are analyzed respectively. Figure 14(a) shows the head vertical acceleration curve of the dummy, it can be seen that the head starts to respond at 6ms, and the head is subjected to the maximum vertical acceleration of 165.9g at about 12 ms, at which time the shock wave produces a greater hazard to the dummy, and the acceleration gradually decays in the time period thereafter, while the HIC_{15} of the dummy's head can be obtained as 138, referring to the head evaluation index in Section 3, it can be seen that the dummy's head is in a safe state. Figure 14(b) shows the synthetic acceleration of the chest of the dummy, and it can be seen that the maximum acceleration generated by the chest is 253.6g, which is far more than the limit value of 60g specified in the corresponding specification for the chest, and it can be seen that the irreversible and huge damage to the chest is generated. From Figure 14(c), it can be seen that the maximum axial compression force on the neck of the dummy at 13 ms was 7.14 kN, which exceeded the specified threshold value of 6.67 by more than 7%. Meanwhile, it can be seen from Figure 14(d) that the maximum value of the neck bending moment of the dummy is 38.2 Nm, which is less than the threshold value of 135 Nm. The neck injury index N_{ij} can be calculated by Formula (2) as 1.35, which exceeds the specified value 1, indicating a high probability of injury caused by external impact on the neck. Figure 14(e) shows the pelvic vertical acceleration curve of the dummy, which responds at 4 ms and peaks at 173.8g at 11 ms due to the impact of the seat, and again peaks at 89.5g at about 38 ms when the dummy falls back into the seat with a secondary impact provided by

the seat. The pelvic acceleration curve can be processed to obtain the thoracolumbar injury index, that is, dynamic response coefficient DRI_z is 17.38, less than the threshold value 17.7, indicating that thoracolumbar is in a safe state. The dummy tibia force data were processed to obtain Figure 14(f). As the foot of the dummy is closest to the deck, it will be transmitted to the tibia immediately after the shock wave. The tibia received a great impact in the first few milliseconds after the explosion, with the force reaching a peak of 20.7 kN (left tibia) and 23.3 kN (right tibia), much higher than the force threshold of the tibia of 5.4 kN. At this time, the tibia of dummy is damaged by high-speed impact. Since the foot of the dummy is in different positions on the deck, the instantaneous acceleration generated by the deck at the two places is different. Therefore, the load transmitted to the tibia through the foot can also make a difference. Figure 14(g) shows the force on the femur of the dummy, which is similar to the force on the tibia. The force on the femur peaks within a few milliseconds of the beginning of the explosion, with a maximum force of 3.34 kN on the left femur and 3.83 kN on the right femur. The second peak is generated by the weak upward motion of the femur due to the acceleration exerted by the deck when the dummy was removed from the seat and returned to the deck again.
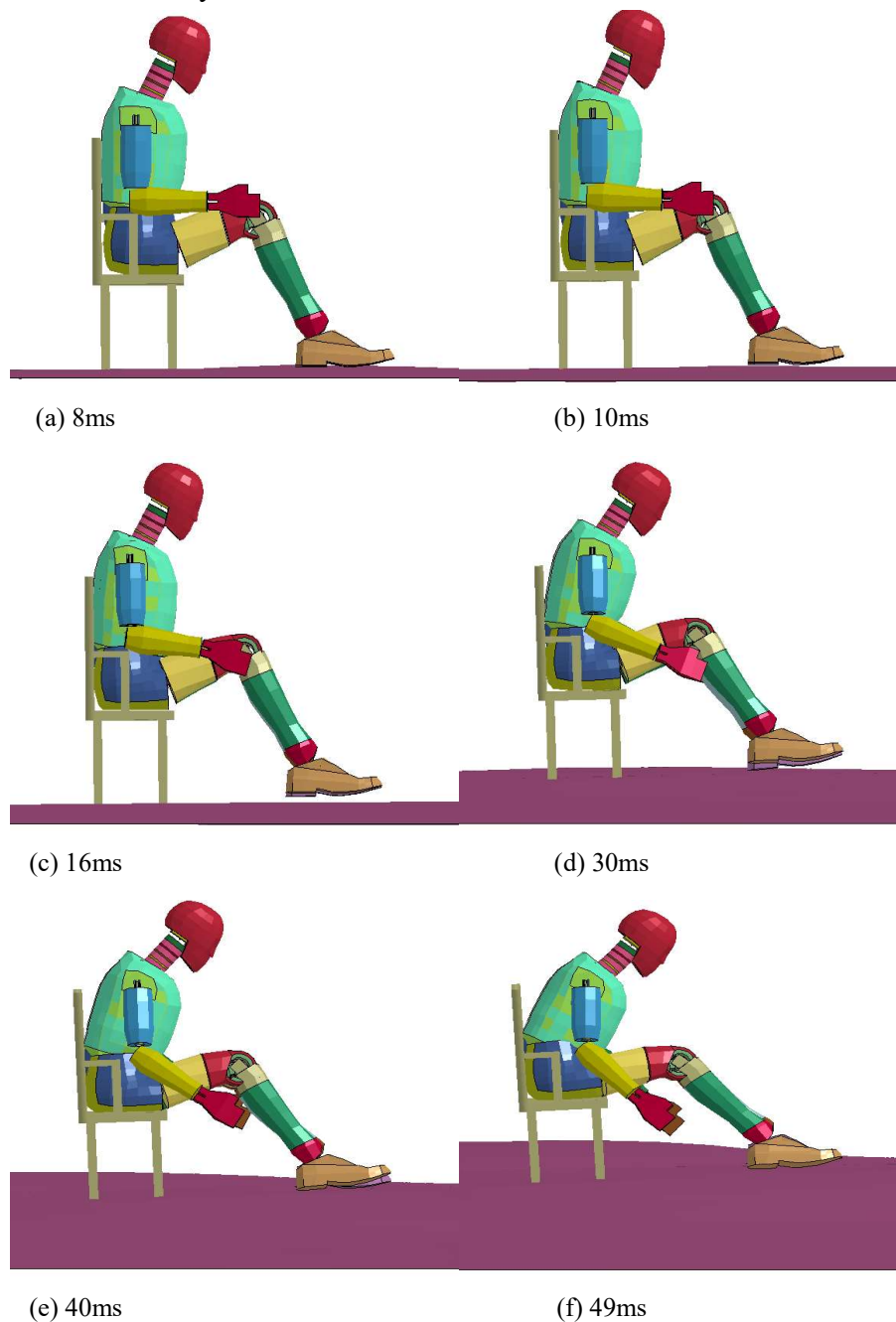
(a) 8ms

(b) 10ms

(c) 16ms

(d) 30ms

(e) 40ms

(f) 49ms

Fig. 13 Posture changes of the dummy at different moments

(a) Z-directional acceleration of head

(b) Chest synthetic acceleration

(c) Neck axial force

(d) Neck axial bending moment

(e) Pelvis z-direction acceleration
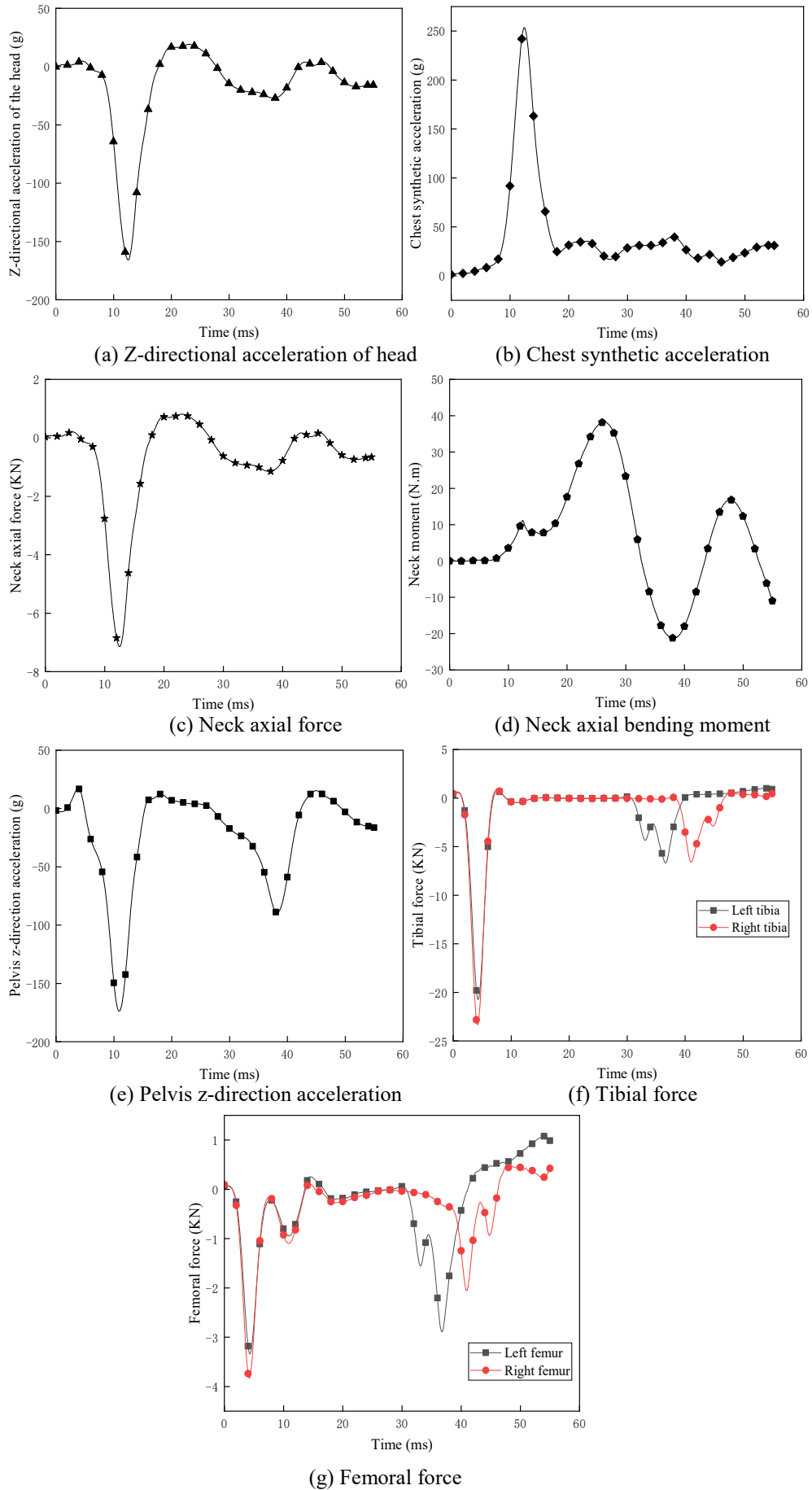
(f) Tibial force

(g) Femoral force

Fig. 14 Damage curve of each part of the dummy in the initial posture

17

4.3 Injury analysis of changing joint angle posture

In order to analyze the effects of vertical impact on the crew under different posture, reasonable angle adjustment is made for each joint of the crew. The posture of the dummy is adjusted and analyzed with reference to ergonomics. At the same time, due to the small difference in force between the left and right sides of the tibia and femur of the crew, in order to facilitate the statistical analysis below, the mean values of the forces on the left and right sides are taken for description.

4.3.1   Change the angle posture between foot and tibia

Change the posture between the dummy's foot and the tibia, and adjust it within the initial angle (110º). Since the dummy's foot is initially parallel to the deck and the maximum stretch value has been reached between the tibia and the foot, the angle between the two can only be reduced, and then the analysis is calculated in turn. In order to obtain the impact of various postures more intuitively on the injury of the dummy, the polar values of the main injury sites are plotted by orthogonal point plots, as shown in Figure 15. As can be seen from Figure 15 (a), the head injury values of the dummy are within the threshold value of 250 and are in a safe condition under the change of foot posture, indicating that the direct impact of the deck impact on the head by the foot is small. Figure 15 (b) shows the neck injury coefficient and neck axial force of the dummy. The neck injury coefficient of the dummy under this condition exceeds the threshold value of 1, and the neck axial force hovers around 7.15 kN, which exceeds the threshold value by more than 7%, thus it can be seen that changing the posture of the foot and tibia does not reduce the neck injury of the dummy. Figure 15 (c) represents the value of acceleration damage to the dummy's chest. With the changed foot posture, the chest acceleration is reduced compared to the initial posture, and the chest acceleration of the dummy gradually decreased as the angle between the foot and the tibia decreased. In the Angle position from 100º to 105º, the dummy's chest angular velocity decreased significantly. Figure 15 (d) shows the thoracolumbar injury value (DRI_Z) of the dummy, which does not exceed the DRI_Z threshold value of 17.7 in all different foot postures, and is in a relatively safe state. The 95º-110º angle posture formed by the foot and tibia has no direct effect on the thoracolumbar spine and presents a smaller DRI_Z value when in the 105º posture. The injury values for the tibia and femur of the dummy in Figure 15 (e) reveal that the load generated by the underwater explosion causes a large injury to the tibia of the dummy's lower leg, far beyond the threshold range of the tibia. The femur bears a load of about 3 kN, and it can be seen that the damage to the femur and tibia is minimal when the dummy foot posture is maintained near 100º. Figure 15 (f) shows the ratio of the damage value of each part of the dummy to the corresponding threshold, and the figure indicates whether the parts are in a safe or damaged state. In addition, when the foot posture is 95º and 105º, the two values are equivalent, and the curves are approximately identical. From the overall trend of all the curves, only the head and the thoracolumbar spine are completely safe for the statistical injury sites, the neck is at the edge of risk, and the rest of the sites have injury values greater than the threshold.

4.3.2   Change the angle posture of femur and tibia

In order to obtain the effect of changes in the tibial and femoral postures of the dummy on the injury of the dummy, reasonable adjustments were made in the initial posture (90º), and separate computational analyses were performed. The analysis was performed in a similar way as in section 4.2.1. As can be seen from Figure 16, as the included angle between the femur and tibia of the dummy increases, HIC_{15} of head injury, N_{ij} of neck injury, CSI of chest and tibial force of dummy all showed a gradually decreasing trend. Only the thoracolumbar injury parameter DRI_Z first increased and then decreased. It can also be seen in Figure 16(f) that the injury ratio at each site is minimal at an angle of 100º between the tibia and the femur. Among all the parts analyzed, the tibia has the largest ratio of force to tolerance values, indicating that the dummy tibia suffered the greatest value of damage, almost irreparable damage, in different femoral and tibial postures, as well as damage to the soft tissues surrounding the tibia, which is of great harm to the crew. In Figure 16(b), the neck injury factor N_{ij} decreases continuously with increasing femoral bending angle, but all

exceed the specified value of 1 and meet the injury criteria. The change pattern of the axial force at the neck of the dummy is not obvious, but in general, as the angle increased, the axial force also increased, and all exceeded the neck axial force threshold of 6.8. As can be seen in Figure 16(e), the load on the femur is opposite to the trend of the tibia, and the axial force on the femur tends to increase with the increase of the angle, which aggravates the injury of the dummy.
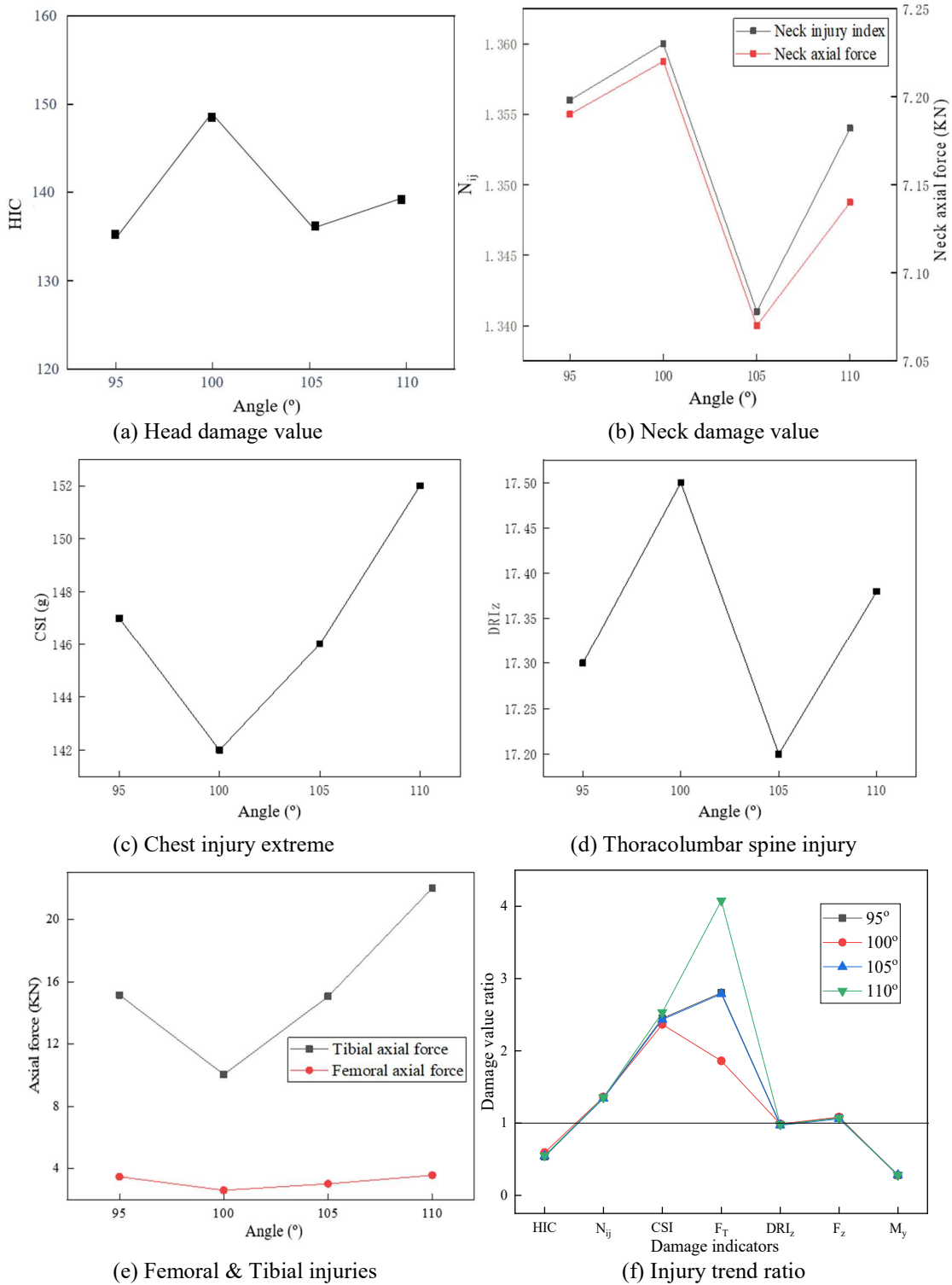

(a) Head damage value

(b) Neck damage value

(c) Chest injury extreme

(d) Thoracolumbar spine injury

(e) Femoral & Tibial injuries

(f) Injury trend ratio

Fig. 15 Injury curve of the foot and tibia in different positions

(a) Head damage value

(b) Neck damage value

(c) Chest injury extreme

(d) Thoracolumbar spine injury

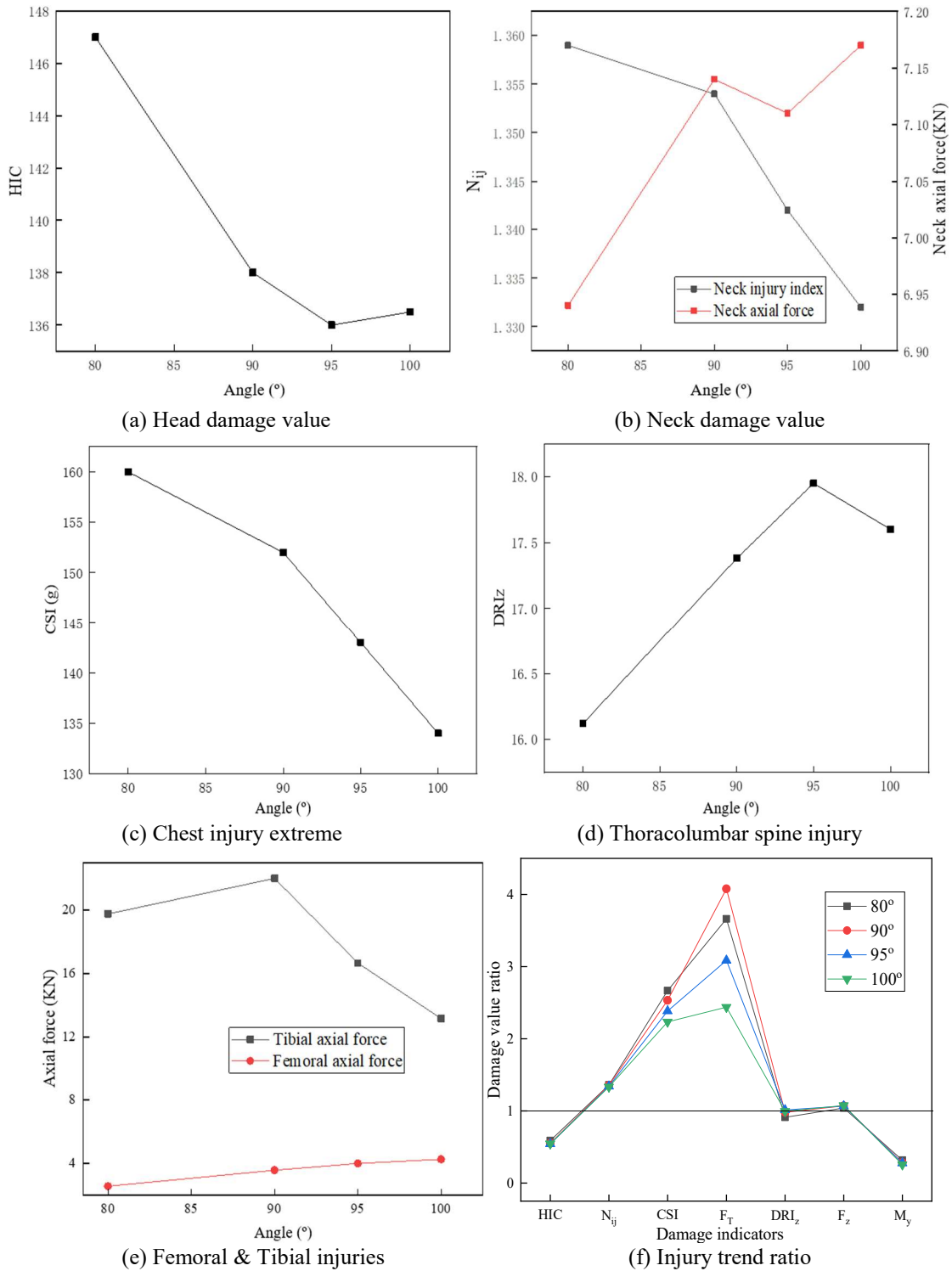(e) Femoral & Tibial injuries

(f) Injury trend ratio

Fig. 16 Injury curves of the tibia and femur in different positions

4.3.3   Change the angle posture between femur and waist

The femur and waist posture of the dummy were changed on the basis of the initial posture (70º), and then calculated and analyzed in turn. As can be seen from Figure 17, the trend of head, neck, thoracolumbar spine, and tibia injuries of the dummy in different postures at this site are consistent, and all showed peak injury values at the posture of 75º. The thoracolumbar injury value of the dummy in the 75º position reached 19.48, exceeding the injury threshold of 17.7, at which point the dummy suffered irreversible damage to the thoracolumbar spine. In contrast, changes in thoracic injuries showed the opposite trend to changes in other sites. From Figure 17(c), it can be seen that the chest acceleration of the dummy decreases continuously with

the increase of angle, indicating that the increase of femoral and waist posture has a significant improvement on the cushioning of the dummy's chest. As can be seen by Figure 17(f), the trend of change in the ratio of injury values corresponding to each angle is consistent for the four postures formed by the femur and the waist, and a comprehensive comparison of the four curves shows that the injury to each part of the dummy is relatively small at the posture of 80º. It can be seen that the dummy is in good condition at 80º posture, which can reduce the damage of explosion shock to the crew. It can provide reference for the femur and waist posture of the crew on the ship. In the event of harm, being in the self-protection posture in advance can reduce the damage caused by external impact.
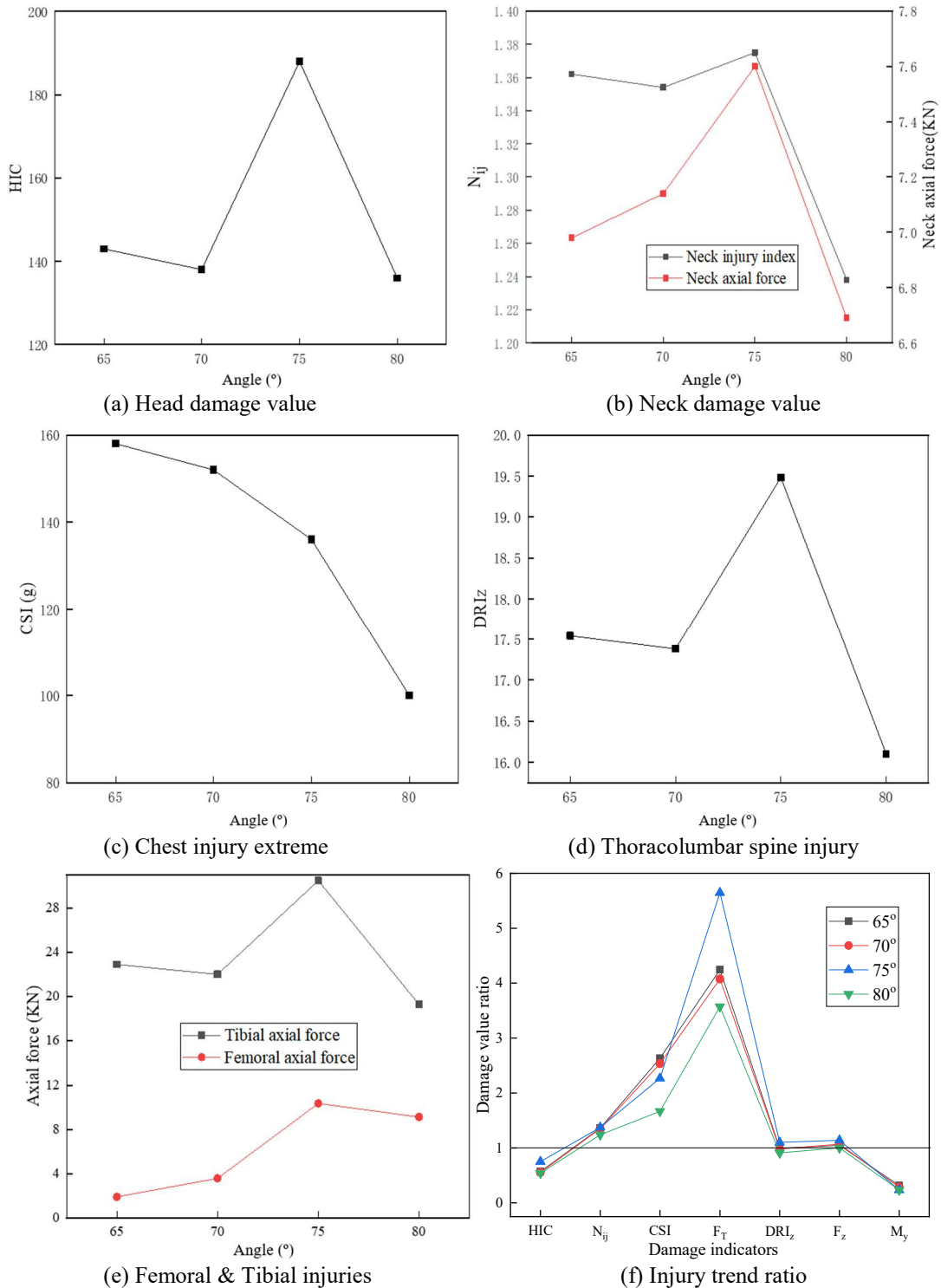

(a) Head damage value

(b) Neck damage value

(c) Chest injury extreme

(d) Thoracolumbar spine injury

(e) Femoral & Tibial injuries

(f) Injury trend ratio

Fig. 17 Femoral and lumbar injury curves in different positions

4.3.4   Change the angle between waist and elbow

In order to observe the influence of changes in the waist and elbow of the dummy on the injury of the dummy, the initial posture (0°) was adjusted and analyzed in turn. According to the analysis of posture injury data of the dummy at different waist and elbow angles, changing the angle of the site can significantly improve the impact of the injury on the dummy, but it has little effect on the dummy beyond a certain range. When the angle between the waist and elbow is 10° and 15°, the injury values of the dummy's head, neck, chest, and thoracolumbar spine are the same, and the subsequent continuation of increasing the angle of the part has no significant effect on the injury values of the dummy.
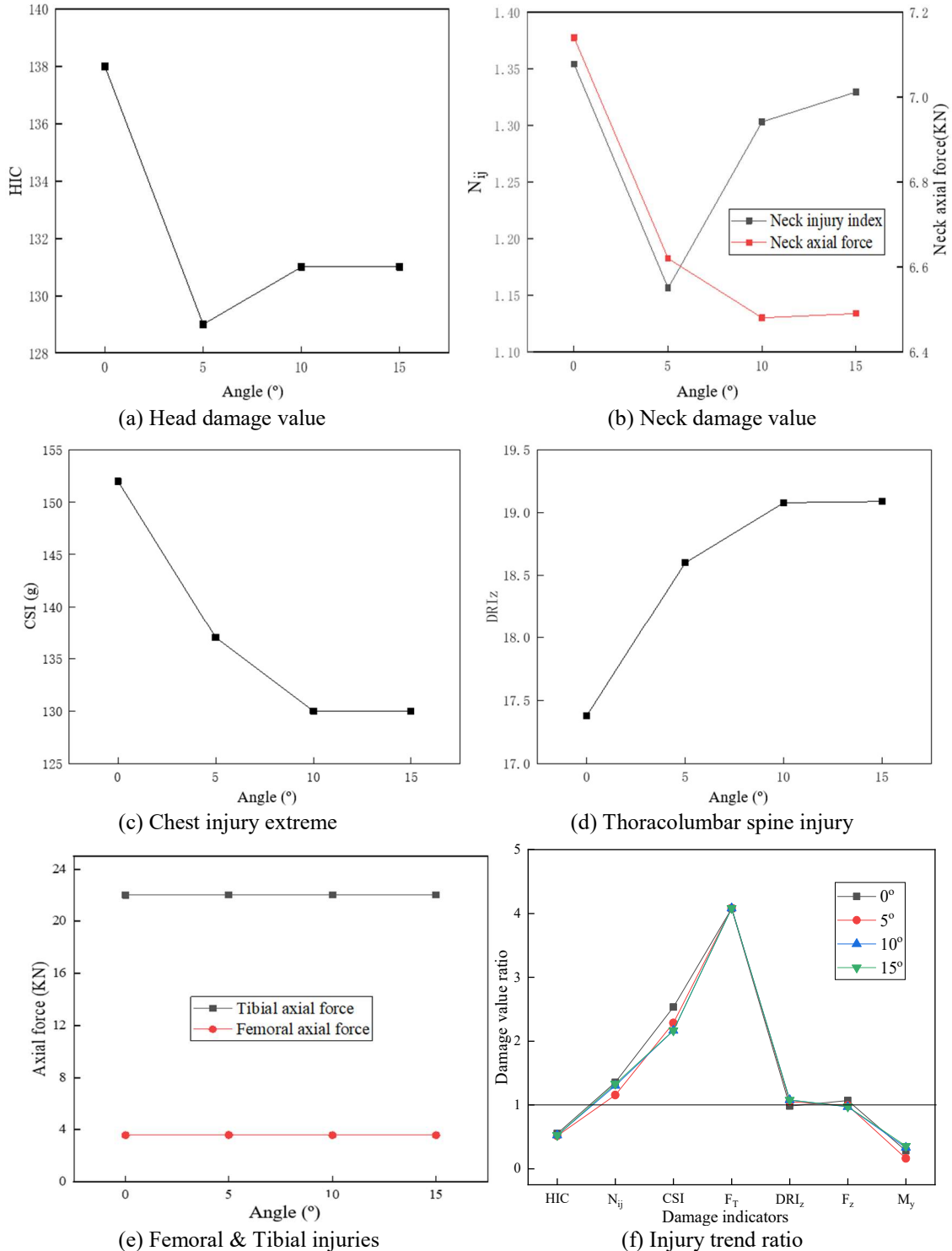

(a) Head damage value

(b) Neck damage value

(c) Chest injury extreme

(d) Thoracolumbar spine injury

(e) Femoral & Tibial injuries

(f) Injury trend ratio

Fig. 18 Injury curves of the lumbar region and elbow in different position

Meanwhile, according to the data distribution in Figure 18(e), changing the posture of the waist and elbow of the dummy has almost no effect on the damage of the femur and tibia. Under the four working conditions of this part, the calculated axial force is the same (the axial force of the tibia is 22.04 kN and the axial force of the femur is 3.59 kN). However, increasing the position of this part can effectively reduce the damage of the shock wave to the head and neck. As can be seen by Figure 18(d), changing the posture of the dummy waist and elbow has a greater impact on the thoracolumbar spine, and when the posture of this part is 0o, the thoracolumbar injury value is less than the tolerance threshold, but as the angle increases, the thoracolumbar injury value rises continuously, and after 5° the corresponding thoracolumbar threshold is much greater than the extreme value of 17.7. In addition, as can be seen from Figure 18(f), the posture change of the dummy's waist and elbow has little change in the threshold ratio of the injured site, and the injury performance is similar under the four angles.

4.3.5   Change the angle between elbow and wrist

The initial posture (90°) of the dummy's elbow and wrist were changed according to ergonomics, and then calculated and analyzed. According to the analysis of the injury data of the dummy, when the dummy changed the posture between the elbow and the wrist, the two parts of the femur and the tibia produced the same injury effect, the axial force of the femur is 3.59 kN and the axial force of the tibia is 22.04 kN. It is shown that the ship in the event of an underwater explosion, changing the position of the upper torso (elbow, wrist) has no effect on the damage to the tibia and femur parts of the dummy, and other protective measures are needed to effectively protect the arm and other parts. Meanwhile, the effective damage ratio of each part under several working conditions of changing the angle posture of elbow and wrist is like the trend when changing the angle posture of waist and elbow, which is better illustrated in Figure 19(f) and Figure 18(f). Under the four conditions of changing the elbow and wrist angle posture, the head injury of the dummy first decreases and then remains unchanged, indicating that the effect on the head of the dummy disappears after increasing the elbow and wrist posture to 100°, which can be verified in Figure 19(a). From Figure 19(b) and Figure 19(d), both the neck injury and thoracolumbar injury of the dummy increased with the increase of elbow and wrist posture, and the injury value of the thoracolumbar injury of the dummy exceeded the injury limit at 110° posture. In contrast, the trend of injury changes in the thorax is the opposite, the acceleration of the thorax gradually decreases with the increase of the included angle, and the increase of the included angle promotes the injury of the thorax, which is better corroborated by Figure 19(c).
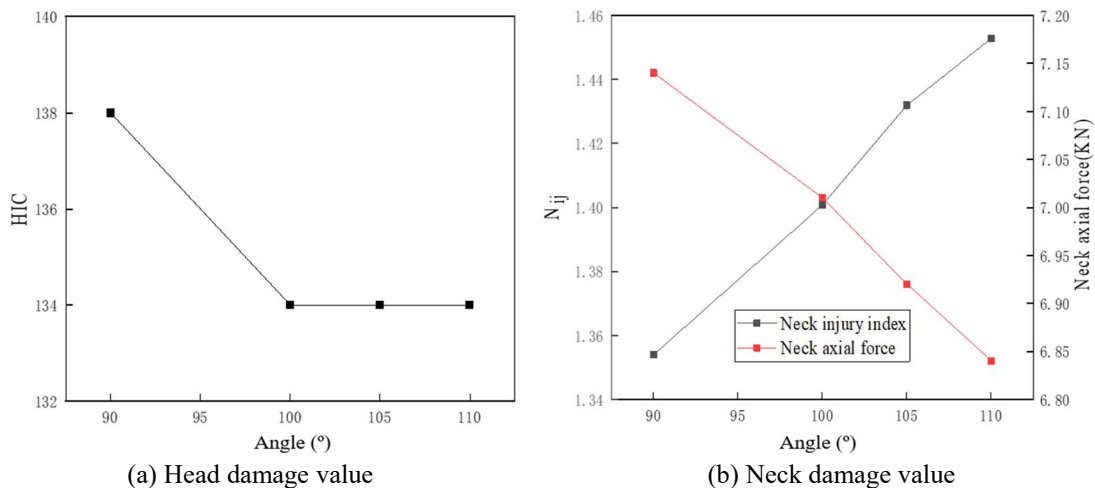

(a) Head damage value   (b) Neck damage value

Fig. 19 Injury curves of the elbow and wrist in different positions

(c) Chest injury extreme

(d) Thoracolumbar spine injury

(e) Femoral & Tibial injuries
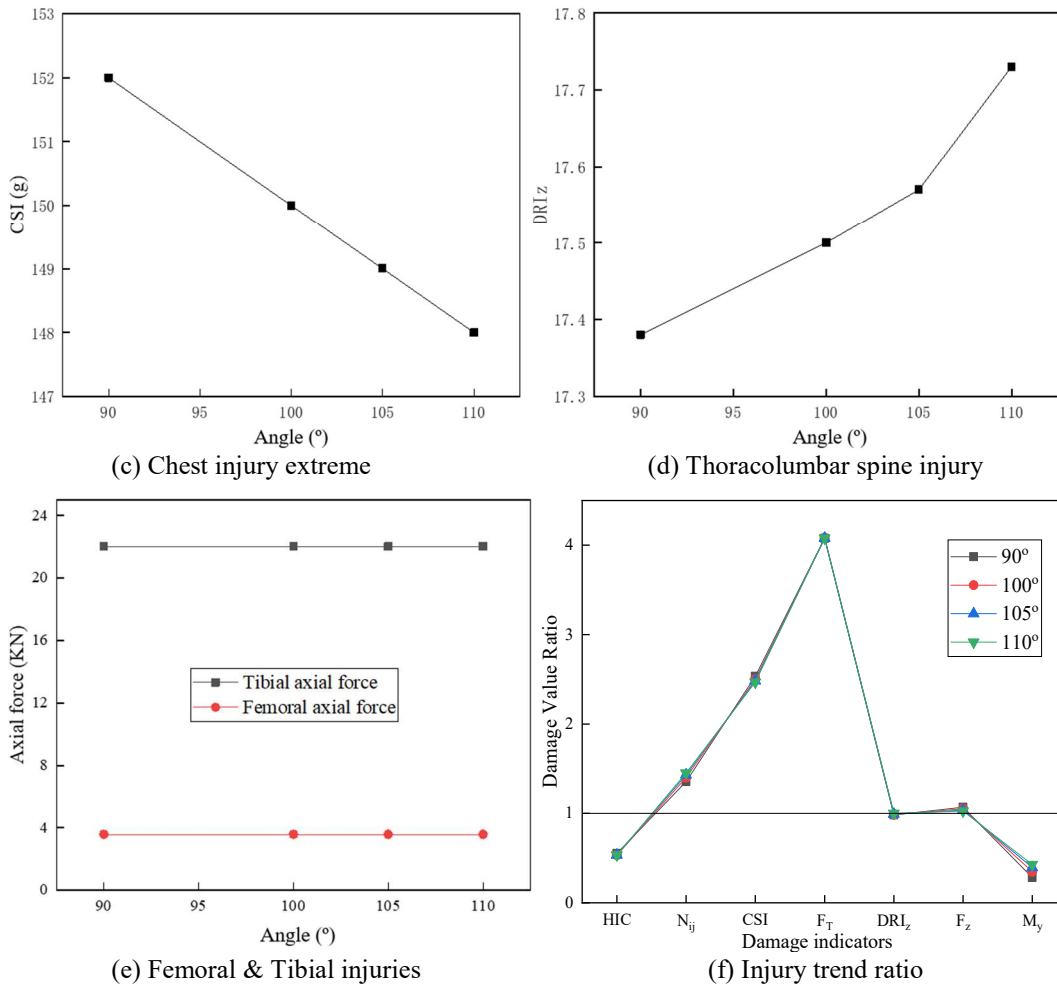
(f) Injury trend ratio

Fig. 19 (continued)

4.4 Analysis of constrained local joint posture injury

4.4.1 Analysis of the impact of foot restraint on the dummy

On the basis of the initial posture of the model, the foot restraint is applied to the dummy to simulate the crew foot protection device, and the damage response after the dummy foot restraint under the same working conditions is explored. Table 8 shows the injury results for each key site after restraint of the dummy foot. It can be seen that the restraint applied to the dummy foot can significantly reduce the damage value of each part and delay the appearance of the peak of each part, which has a protective effect on the crew to some extent. The head injury value (HIC_{15}) is reduced by 80, 58% compared with the same period, the neck injury coefficient N_{ij} is reduced to a safe range, the chest acceleration is reduced by 39.5%, the dynamic response coefficient DRI_Z is reduced by 47.8%, the femur force is reduced by about 1 kN, 27.6%, and the tibia force is reduced by 18.37 kN, a reduction of 83.5%, indicating that the foot constraint played a better role in protecting the tibia of the dummy. Meanwhile, the peak neck axial force of the dummy is reduced by 3.96 kN, or 55.5%, the neck moment is reduced by 27.8%. Among all the damaged sites counted, only the chest compression showed an increasing trend with an increase of 4.15 mm. As can be seen from Figure 20, this is due to the foot restraint, the impact generated by the explosion, the dummy mainly through the seat to the pelvis upward load, so that the dummy in the case of the foot remains motionless only the movement of the pelvis drives the displacement of the upper torso of the dummy, the thighs have a small deformation of movement. Currently, the head, neck and chest of the dummy tend to lean forward, and in the process of

movement, the dummy's neck drives the head down due to inertial forces and gravity, which exacerbates the risk of injury to the chest, resulting in an increase in chest compression.

Table 8 Foot restraint dummy impairment values

	HIC	N_{ij}	CSI (g)	$DRIz$	F_E (kN)	F_T (kN)	M_y (kNmm)	F_Z (kN)	Comp (mm)
Foot Restraint	58.00	0.68	92.00	9.08	2.60	3.64	27.61	3.18	9.00

Fig. 20 Effect of injury after dummy foot restraint

4.4.2 Analysis of the influence of tibial restraint on dummy

A constraint is applied to the tibia of the lower leg of the dummy based on the original model to investigate the effect of limiting only the motion of the tibia on the injury response of the crew under the same working conditions. The numerical simulation results are shown in Table 9. Through analysis and comparison of the injury data, it can be seen that limiting the movement of the dummy's lower leg and tibia increased the damage value of the dummy's key parts. Among them, the injury values of the head, neck, femur, tibia and thorax of the dummy increased compared with the injury values of the original model, especially the force on the tibia is much higher than the tolerance limit of the area, indicating that the tibia has reached the injury risk level of fatal injury, which has a fatal impact on the state of the dummy. The rest of the parts only chest acceleration, dynamic response coefficient of thoracolumbar spine, axial force of the neck these indicators have buffered the decline, the overall restriction of the dummy tibia movement will aggravate the damage value of each part, is not conducive to the survival of the crew in the explosion environment. Meanwhile, it can be seen from Figure 21 that after restraining the tibia, the dummy will have an upward movement trend under the acceleration impact provided by the seat. Due to the limitation of the tibia, the lower torso of the dummy remains almost immobile, and the foot of the dummy will flip upward under the impact of deck acceleration, and the angle with the tibia continues to decrease, which will seriously damage the soft tissues near the ankle and cause irreparable damage. Therefore, limiting the movement of the dummy tibia is not desirable in an underwater explosion.

Table 9 Impairment values for tibial restraint dummies

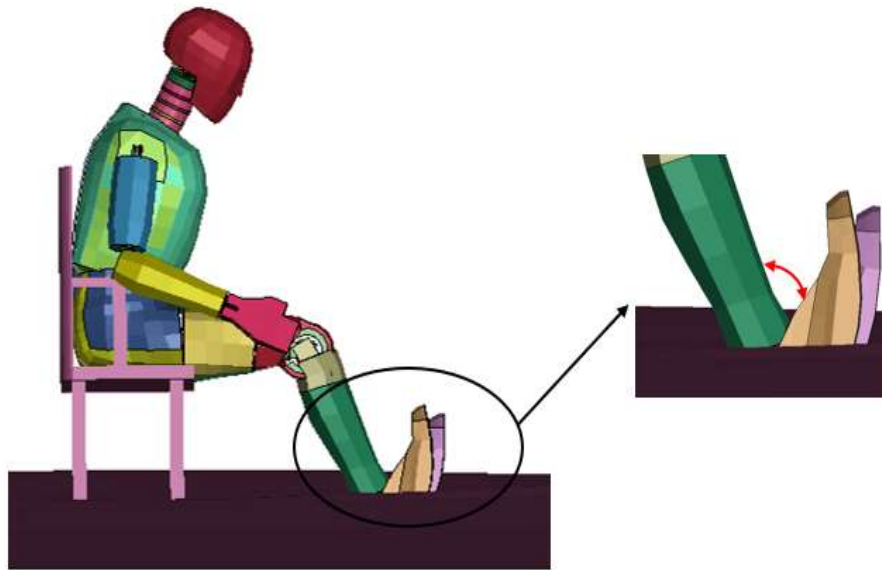|	HIC	N_{ij}	CSI (g)	$DRIz$	F_E (kN)	F_T (kN)	M_y (kNmm)	F_Z (kN)	Comp (mm)
Foot Restraint	142	1.17	137	14.34	49.37	427.12	52.34	5.2	20.25

Fig. 21 Effect of injury after tibial restraint in dummy

4.5 Analysis of variation range of damage value under various postures

In order to study the range of variation of the standard values of dummy damage, this paper tries to relate the damage values to the dummy posture parameters. The damage data and joint angles of each key part of the dummy are plotted separately in the form of Figure 22, the angles in the figure represent the joint angle values under different postures. According to the data statistics, only the injury data of the head, thoracolumbar spine, chest and tibia showed strong density in the posture angles of different parts, while there is no obvious correlation between other injury data and postural parameters, and the data distribution is scattered.
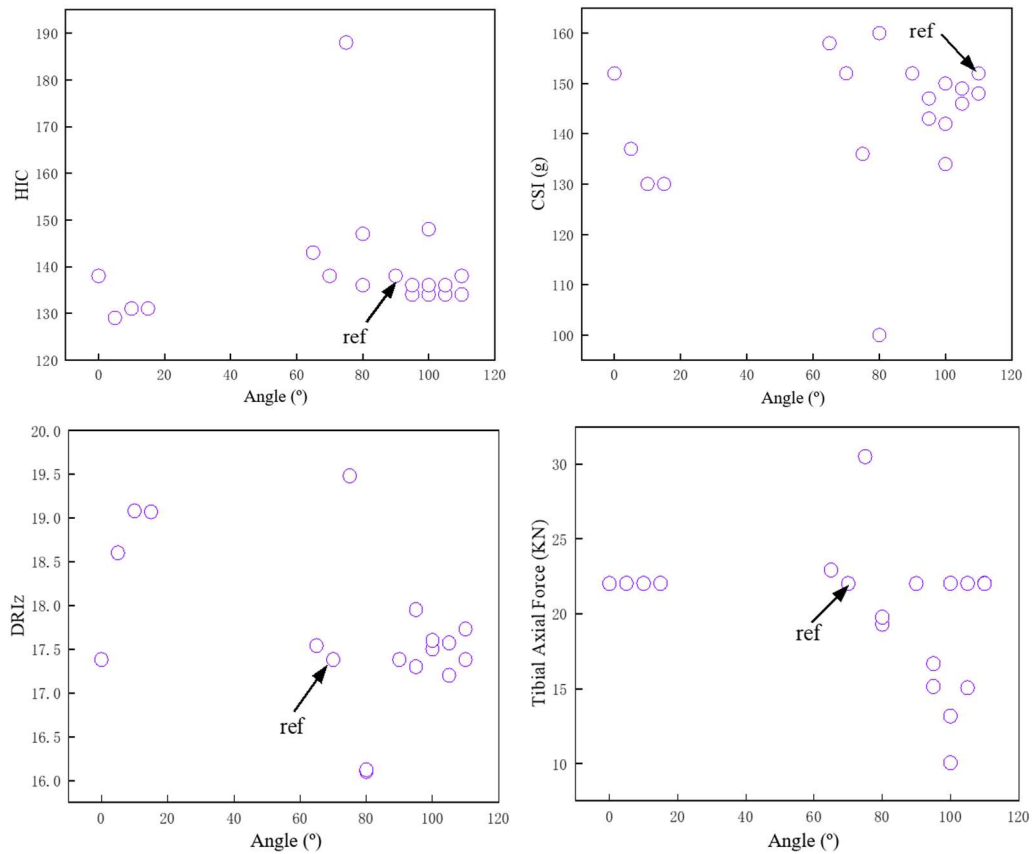

Fig. 22 Distribution of injury data

26

From Figure 22, the head injury (HIC_{15}) range corresponding to various postures of the dummy is 129-143, and the reference value of head injury in the initial posture is 138. The damage range of chest acceleration (CSI) is 134g-153g, and the reference value of chest acceleration damage under initial posture is 152g. The dynamic response coefficient (DRI_Z) corresponding to the thoracolumbar spine ranges from 17.2-17.95, with a reference value of 17.38 for the dynamic response coefficient in the initial posture. The tibial axial force injury range is 19kN-23 kN, and the reference value of the lower leg tibial force in the initial posture is 22 kN. The above analysis mainly analyzes the damage concentration value of the key parts of the dummy under the same working condition, and provides certain reference for the damage of the dummy with different posture under the corresponding working condition.

5. Explosives equivalent to the crew damage and high risk of injury site analysis

5.1 Different explosive equivalents on the impact of crew damage

In order to analyze the effects of different explosive equivalents on crew damage at the same detonation distance, increase or decrease by 50 kg based on 100 kg TNT, calculate the explosive equivalent conditions of 50 kg TNT and 150 kg TNT respectively, and analyze the results of damage to crew. The computations under varied explosive weights consistently exhibit hull deformation and petal-shaped breach near the explosion source. As the explosive scales up, the hull bottom breach gradually deepen, with increasingly severe overall deformations.

Table 10 shows the damage values for each part under the three working conditions. Each damage parameter in the table shows an increasing trend with the increase of explosive equivalents. Meanwhile, the damage curve analysis shows that with the increase of explosive equivalents, the damage data of each part appears peak in advance, indicating that the increase of explosive equivalents will trigger the dynamic response of the dummy in advance. Therefore, the explosive equivalent of the damage to the dummy in the underwater explosion has a greater impact, the less the amount of explosives, the smaller the damage parameters of the various parts of the dummy, the lower the overall damage state, the lower the probability of being at risk. Conversely, the higher the probability of damage caused by the impact of the dummy.

Table 10 Corresponding damage values of the dummy at different explosive equivalents

TNT equivalent	HIC	N_{ij}	CSI (g)	$DRIz$	F_E (kN)	F_T (kN)	M_y (kNmm)	F_Z (kN)	Comp (mm)
50kg	92	0.76	71	5.05	2.72	16.52	30.57	3.54	3.02
100kg	138	1.35	152	17.38	3.59	22.01	38.23	7.14	4.85
150kg	195	1.71	173	28.96	4.18	25.89	46.02	9.16	7.18

Figure 23 represents the damage ratio of each site at three explosive equivalents. The curves of the three explosive equivalents follow the same trend, with the increase of explosive equivalents, the damage ratio greater than 1 gradually increased in the parts. When the dosage is 150 kg, the damage ratio of most parts is more than 1, indicating that the dummy has suffered different degrees of impact damage in the corresponding parts at this time, on the contrary, there are relatively more parts in the safe state. Table 10 and Figure 23 show better the damaged state of the dummy for different explosive equivalent working conditions.
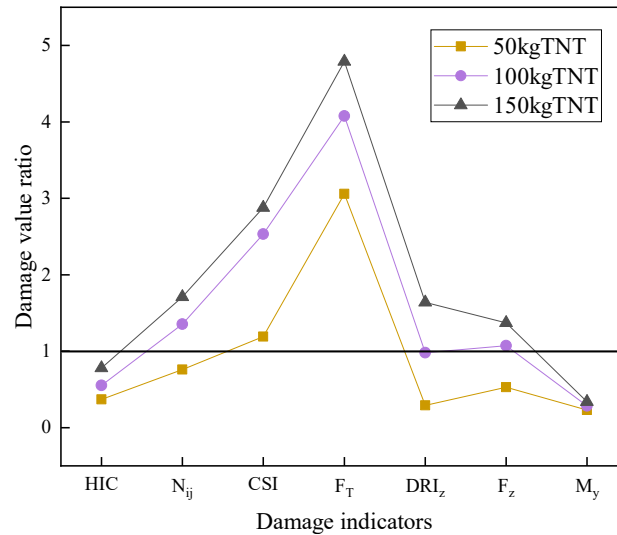
Fig. 23 Corresponding damage ratios for different explosive equivalents

5.2 Analysis of high-risk injury sites

Underwater blast impact mainly through the deck and seat transfer to the crew load, the load in the process of transfer of decay, deck impact on the foot, through the tibia to the femur, in turn, the lumbar spine, chest, neck, head. The impact of the seat mainly acts on the pelvis of the dummy, transmits to the thoracolumbar spine, and finally to the head. Therefore, the parts near the deck and seat have greater damage, and the feet and tibia have the greatest impact, followed by the chest. Similar to the research results [37], the head suffers relatively little damage of all parts, it is far from the impacted part, and the load transfer to the head has occurred several times fold reduction. Analysis of the impact injury results in sections 4 and 5.1 also confirms that the tibia and thorax produced greater injury values and are at a higher probability of being damaged, followed by a higher risk of damage to the neck.

6.   Conclusion

In this paper, a numerical calculation model containing crew, hull structure and flow field is established, and the damage to the main body parts of the crew after the explosion is analyzed based on the destructive effect of the underwater explosion load on the hull structure, and the dynamic response of the crew under the action of the underwater explosion shock wave is analyzed from multiple angles and factors. The main conclusions are as follows:

1) Under the same explosion condition, changing the different joint postures of the dummy will have a certain impact on the damage of other parts of the dummy. However, when changing the posture of different parts of the dummy 's upper body (such as elbow, wrist, etc.), the impact on lower limb injury is small. In the different postures of the statistics, only the head has been in a safe state after the impact of the explosion, and the rest of the parts bear the risk of injury above AIS2 +. In practice, the posture of different parts of the crew can be adjusted to reduce the risk of injury.

2) Restricting the foot joints of the crew in a sitting position through the protection device on the ship can effectively reduce the risk of injury to various parts of the crew, especially the protection of the tibia. However, restricting other parts such as the tibia will increase the probability of injury to the crew.

3) The effect of explosive equivalent on the dummy is positively correlated. The greater the amount of explosive, the damage value of each part of the dummy gradually increases. Under different explosive equivalents, the impact on the crew 's head is the smallest, and the risk of AIS2 + on the tibia is the highest.

REFERENCES

[1]   O'Daniel, J.L., Koudela, K.L., Krauthammer, T., 2005. Numerical Simulation and Validation of Distributed Impact Events. *International Journal of Impact Engineering*, 31(8), 1013-1038. https://doi.org/10.1016/j.ijimpeng.2004.06.002

[2]   Li, L., Feng, S., Jiang, J., 2007. Numerical Simulation of Damage Effect on the Bottom Construction of a Ship Subjected to Underwater Explosion. *Proceedings of the 7th International Conference on Shock & Impact Loads on Structures*, 17-19 October, Beijing, China, 343-348.

[3]   Chung, J., Seo, Y., Shin, Y.S., 2020. Dynamic and Whipping Response of the Surface Ship Subjected to Underwater Explosion: Experiment and Simulation. *Ships and Offshore Structures* 15(10), 1129-1140. https://doi.org/10.1080/17445302.2019.1706924

[4]   He, Z., Chen, Z., Jiang, Y., Cao, X., Zhao, T., Li, Y., 2020. Effects of the Standoff Distance On Hull Structure Damage Subjected to Near-Field Underwater Explosion. *Marine Structures,* 74, 102839. https://doi.org/10.1016/j.marstruc.2020.102839

[5]   Mannacio, F., Barbato, A., Di Marzo, F., Gaiotti, M., Rizzo, C.M., Venturini, M., 2022. Shock Effects of Underwater Explosion on Naval Ship Foundations: Validation of Numerical Models by Dedicated Tests. *Ocean Engineering,* 253, 111290. https://doi.org/10.1016/j.oceaneng.2022.111290

[6]   Geers, T., 1978. Doubly Asymptotic Approximations for Transient Motions of Submerged Structures. *Journal of the Acoustical Society of America,* 64(5), 1500-1508. https://doi.org/10.1121/1.382093

[7]   Gupta, N.K., Kumar, P., Hegde, S., 2010. On Deformation and Tearing of Stiffened and Un-Stiffened Square Plates Subjected to Underwater Explosion−a Numerical Study. *International Journal of Mechanical Sciences,* 52(5), 733-744. https://doi.org/10.1016/j.ijmecsci.2010.01.005

[8]   Sprague, M.A., Geers, T.L., 2006. A Spectral-Element/Finite-Element Analysis of a Ship-Like Structure Subjected to an Underwater Explosion. *Computer Methods in Applied Mechanics and Engineering,* 195(17-18), 2149-2167. https://doi.org/10.1016/j.cma.2005.03.007

[9]   Bose, D., Crandall, J.R., Untaroiu, C.D., Maslen, E.H., 2010. Influence of Pre-Collision Occupant Parameters on Injury Outcome in a Frontal Collision. *Accident Analysis & Prevention*, 42(4), 1398-1407. https://doi.org/10.1016/j.aap.2010.03.004

[10]   Zhou, D., Wang, X., Zhou, Y., Sun, X., 2019. Comparison of Numerical Approaches for Modeling a Scaled Underbelly Structure Subjected to Landmine Impulse. *Shock Waves*, 29(4), 573-582. https://doi.org/10.1007/s00193-018-0869-2

[11]   Lam, K.Y., Zong, Z., Gong, S.W., 1999. Human Exposure to Underwater Shock Modeling and Simulation. *Proceedings of the Naval Technology Seminar Platform*.

[12]   Zong, Z., Lam, K.Y., 2002. Biodynamic Response of Shipboard Sitting Subject to Ship Shock Motion. *Journal of Biomechanics,* 35(1), 35-43. https://doi.org/10.1016/S0021-9290(01)00167-1

[13]   Orłowski, M., Bastien, C., Razmkhah, O., Mccartan, S. 2017. Design Methodology for Crash Occupant Protection in Cabin Design of the High Speed Vessel. *Marine Structures,* 51, 1-20. https://doi.org/10.1016/j.marstruc.2016.10.001

[14]   North Atlantic Treaty Organization AEP-55. 2011. Procedures for Evaluating the Protection Level of Armored Vehicles-Mine Threat: Volume 2 (Edition 2). *Allied Engineering Publication*.

[15]   North Atlantic Treaty Organization TR-HFM-090. 2007. Test Methodology for Protection of Vehicle Occupants against Anti-Vehicular Landmine Effects: Final Report of HFM-090 Task Group 25. *AGARD & RTO publications*.

[16]   Mertz, H.J., Hodgson, V.R., Thomas, L.M., Nyquist, G.W., 1978. An Assessment of Compressive Neck Loads Under Injury-Producing Conditions. *Physician Sportsmed,* 6(11), 95-106. https://doi.org/10.1080/00913847.1978.11948406

[17]   Prasad, P., Roger P.D., 1984. A Biomechanical Analysis of Head, Neck, and Torso Injuries to Child Surrogates Due to Sudden Torso Acceleration. *SAE Transactions*, 784-799. https://doi.org/10.4271/841656

[18]   Marc, B., Nicholas, S., Newmanâ, J.A., 2002. Head, Neck, and Body Coupling in Reconstructions of Helmeted Head Impacts. *Proceedings of the 2001 International IRCOBI Conference on the Biomechanics of Impact,* Isle of Man, UK, 295-310.

[19]   Eppinger, R., Sun, E., Bandak, F., Haffner, M., Khaewpong, N., Maltese, M., Kuppa, S., Nguyen, T., Takhounts, E., Tannous, R., Zhang, A., Saul, R., 1999. Supplement: Development of Improved Injury Criteria for the Assessment of Advanced Automotive Restraint Systems - II. *National Highway Traffic Safety Administration Vehicle Research & Test Center (VRTC)*.

[20]   Stech, E.L., A Payne, P.R., 1969. Dynamic Models of the Human Body. *Engineering*. https://doi.org/10.21236/AD0701383

[21]   Yoganandan, N.P., Kumaresan, S.M., Voo, L.P., Pintar, F.A.P., 1996. Finite Element Applications in Human Cervical Spine Modeling. *Spine*, 21(15), 1824-1834. https://doi.org/10.1097/00007632-199608010-00022

[22]   Morgan, R.M., Eppinger, R.H., Marcus, J.H., Nichols, H., 1990. Human Cadaver and Hybrid III Responses to Axial Impacts of the Femur. *The 1990 International IRCOBI Conference on the Biomechanics of Impact,* 12-14 September, Bron-Lyon, France, 21-35

[23]   Hui, L., Zhiyong, S., Bingbing, H., Yuhang, S., Baoli, D., 2022. Research on the Motion Response of Aquaculture Ship and Tank Sloshing Under Rolling Resonance. *Brodogradnja*, 73(2), 1-15. https://doi.org/10.21278/brod73201

[24]   Hadi, E.S., Tuswan, T., Azizah, G., Ali, B., Samuel, S., Hakim, M.L., Hadi, M.R.C.P., Iqbal, M., Sari, D.P., Satrio, D., 2023. Influence of the Canal Width and Depth on the Resistance of 750 Dwt Perintis Ship Using CFD Simulation.

Brodogradnja, 74(1), 117-144. https://doi.org/10.21278/brod74107

[25] Mikulec, M., Piehl, H. 2023. Verification and Validation of CFD Simulations with Full-Scale Ship Speed/Power Trial Data. *Brodogradnja*. 74(1), 41-62. https://doi.org/10.21278/brod74103

[26] Szturomski, B., 2015. The effect of an underwater explosion on a ship. *Zeszyty Naukowe Akademii Marynarki Wojennej*. 201(2), 57-73. https://doi.org/10.5604/0860889X.1172074

[27] Huang, S., Jin, Z., Chen, Y., 2021. Underwater blast resistance of double cylindrical shells with circular tube stiffeners. *Ocean Engineering*, 238, 109691. https://doi.org/10.1016/j.oceaneng.2021.109691

[28] Lou, K. A., Bosen, D., Irde, K., Blackburn, Z., 2014. Simulation of Various LSTC Dummy Models to Correlate Drop Test Results. *13th International LS-DYNA User Conference*, 8-10 June, Detroit, USA.

[29] Liu, K., Wang, Z., Tang, W., Zhang, Y., Wang, G., 2015. Experimental and Numerical Analysis of Laterally Impacted Stiffened Plates Considering the Effect of Strain Rate. *Ocean Engineering,* 99, 44-54. https://doi.org/10.1016/j.oceaneng.2015.03.007

[30] Zhang, S., Wang, G., Wang, C., Pang, B., Du, C., 2014. Numerical Simulation of Failure Modes of Concrete Gravity Dams Subjected to Underwater Explosion. *Engineering Failure Analysis,* 36, 49-64. https://doi.org/10.1016/j.engfailanal.2013.10.001

[31] Liu, K., Li, X., Hao, H., Li, X., Sha, Y., Wang, W., Liu, X., 2019. Study on the Raising Technique Using One Blast Based On the Combination of Long-Hole Presplitting and Vertical Crater Retreat Multiple-Deck Shots. *International Journal of Rock Mechanics and Mining Sciences,* 113, 41-58. https://doi.org/10.1016/j.ijrmms.2018.11.012

[32] Wei, X.Y., Zhao, Z.Y., Gu, J., 2009. Numerical Simulations of Rock Mass Damage Induced by Underground Explosion. *International Journal of Rock Mechanics and Mining Sciences,* 46(7), 1206-1213. https://doi.org/10.1016/j.ijrmms.2009.02.007

[33] Lee, E.L., Hornig, H.C., Kury, J.W., 1968. Diabatic Expansion of High Explosive Detonation Products. *University of California Radiation Laboratory at Livermore*, Livermore, CA (United States). https://doi.org/10.2172/4783904

[34] Banadaki, M.D., 2011. Stress-Wave Induced Fracture in Rock Due to Explosive Action. *University of Toronto, Scarborough*, Canada.

[35] Martinez, L., Vicente, T., García, A., Alcalá, E., Izquierdo, F., 2009. Analysis of Coaches Rows Seats Distance Influence on the Passengers Comfort and Safety. *National Highway Traffic Safety Administration*.

[36] Sielicki, P.W., Gajewski, T., 2019. Numerical Assessment of the Human Body Response to a Ground-Level Explosion. *Computer Methods in Biomechanics and Biomedical Engineering.* 22(2), 180-205. https://doi.org/10.1080/10255842.2018.1544628

[37] Jiang, Y., Cao, X., Wang, Y., Wu, C., Li, Y., 2021. Response of Seated Human Subject to Ship Structure Motion Caused by the Combined Effect of Shock Wave and Bubble Pulsation. *Journal of Biomechanics,* 127, 110666. https://doi.org/10.1016/j.jbiomech.2021.110666